

---

## Monosynaptic inference via finely-timed spikes

Jonathan Platkiewicz · Zachary Saccomano ·  
Sam McKenzie · Daniel English · Asohan  
Amarasingham

**Abstract** Observations of finely-timed spike relationships in population recordings are often used to support partial reconstruction of neural microcircuit diagrams. Here fine-timescale components of paired spike train interactions are isolated and subsequently attributed to synaptic parameters. Recent perturbation studies strengthen the case for such inferences, yet the complete set of measurements needed to calibrate statistical models are unavailable. To address this gap, we study features of pairwise spiking in a large-scale *in vivo* dataset where presynaptic neurons were explicitly decoupled from network activity by juxtacellular stimulation. We then develop biophysical models of paired spike trains to reproduce the phenomenology of monosynaptic interactions observed in those data, including both fine-timescale spike-spike correlations and the irregular firing found *in vivo*. We use simulated data generated from these biophysical models to study the inference of small synaptic changes from spike data, despite the presence of rapidly-varying background network fluctuations. A

---

Jonathan Platkiewicz\*

Department of Mathematics, The City College of New York, The City University of New York, New York, NY 10031, USA

Zachary Saccomano\*

Department of Biology, The Graduate Center, The City University of New York, New York, NY 10016, USA

Sam McKenzie

Neuroscience Institute, New York University, New York, NY 10016, USA

Daniel English

School of Neuroscience, Virginia Tech, Blacksburg, VA 24060, USA

Asohan Amarasingham

Department of Mathematics, The City College of New York, The City University of New York, New York, NY 10031, USA

Departments of Biology, Computer Science, and Psychology, The Graduate Center, The City University of New York, New York, NY 10016, USA

E-mail: aamarasingham@ccny.cuny.edu

\*=These authors contributed equally to this work.

**Acknowledgements.** We thank G. Buzsáki for providing advice and inspiring our work on this problem, and T. Evans, M. Regnaud, and H. Rotstein for advice and comments. This work was supported by NIMH R01-MH102840 (A.A.), DOD ARO W911NF-15-1-0426 (A.A. and J.P.), PSC-CUNY 68521-00 46 (A.A.), and NIMH K99 MH118423 (S.M.). We warmly acknowledge the hospitality of the Initiative for Theoretical Sciences (ITS) at the CUNY Graduate Center.

particular focus is the justification and application of a nonparametric separation of timescale principle, based on conditional inference, to implement synaptic inference. We develop a correspondence between classes of stochastic integrate-and-fire neurons and nonparametric inference in the context of microcircuit inference. A secondary goal is to initiate a critical exploration of neurostatistical assumptions in terms of biophysical mechanisms, particularly with regards to the challenging but arguably fundamental issue of fast, unobservable nonstationarities in background dynamics.

**Keywords** Integrate-and-fire neuron; spike correlogram; noise models; synchrony; synaptic connectivity; nonstationarity

## 1 Introduction

The difficulty of studying brain connectivity in behavioral conditions is a major challenge in systems neuroscience. One approach is to attempt to infer microcircuit diagrams indirectly from large-scale spike population recordings (Fujisawa et al., 2008). A synaptic connection is detected when a spike in a reference neuron is followed, with statistical regularity, by finely-timed spikes in a putative target neuron, with time delays consistent with monosynaptic delays (e.g., 2-3 ms). However, there are alternative explanations for these observations, such as indirect polysynaptic partners as well as common (“third party”) input. In this vein, simultaneous optogenetic or juxtacellular stimulation of small groups of cells permit a partial decoupling of presynaptic neurons from the ongoing network activity in *in vivo* conditions, and have strengthened the justification for such an analysis (English et al., 2017). However, even with the benefit of finely-targeted control, the majority of detectable synaptic connections will require analysis of fine-temporal pairwise spike interactions to dissociate coarsely-timed network co-modulation from synaptically-mediated synchrony. Arguably, the state-of-the-art of such inferences is still *ad hoc*. Most likely, existing methods are valid in the case of strong connections, whereas subtleties in the analysis come into play in the case of transient, weak, or sparsely-active synapses, and may lead to significant errors as recordings scale up (Jun et al., 2017). These problems motivate the establishment of a convincing physiologically-relevant statistical framework for quantifying the evidence for synaptic interactions beyond the role of background co-modulation.

A fundamental statistical issue, then, is how to detect and quantify the presence of finely-timed spikes in the presence of background fluctuations. The issue becomes delicate when, as has been argued in more general terms (Brody, 1999; Marshall et al., 2002; Ventura et al., 2005; Amarasingham et al., 2015; Yu and Ferster, 2013), the background dynamics may be nonstationary and rapidly varying, complicating the preliminary task of accurately estimating their properties. An approach to this problem of estimation has been developed based on a statistical technique called conditional inference (Amarasingham et al., 2012). The key technical idea is that hypotheses regarding fine temporal structure are formulated in terms of conditional probability distributions on spike locations, conditioned on a coarsening of the spike trains. The extent of the coarsening specifies the background timescale. The formulation through conditional distributions allows one to sidestep the estimation problem. The statistical technique of *jittering* spikes at a certain timescale and then studying the effect of this data-analytic perturbation on the temporal structure of a spike train is an intuitive prototype of this computation. The physiological relevance of this technique was supported by its application in several *in vivo* findings: most notably, the recovery from *in vivo* extracellularly recorded spike times of typical *in vitro* short-term plasticity patterns (Fujisawa et al., 2008).

A more precise connection, however, between pairwise spiking data and physiological parameters requires a biophysical interpretation. Several biophysical models of fast monosynaptic dynamics have been proposed, but these largely derive from *in vitro* observations (Herrmann and Gerstner, 2001). Moreover, none of these models reproduce the extremely fine-temporal spike-spike correlations observed *in vivo* (Ostojic et al., 2009) and described above. Here we develop a biophysical model that accounts for these correlations while accommodating two apparently contradictory *in vivo* features: millisecond-precise spiking at a synapse and high firing variability. We use the model to demonstrate the use of the conditional approach to inferring fast monosynaptic interactions. Within this framework, we derive a closed-form equation for inferring an excess synchrony estimate from spike times, and evaluate its characterization of synaptic properties against the biophysical data.

The work serves to confirm the relevance of the conditional modeling approach, while clarifying its critical quantitative assumptions. Challenges associated with biophysical interpretations of the background timescale are highlighted. A related, more general, objective is to contribute to the important conceptual task of reconciling dynamical and statistical levels of neurophysiological description (Kass et al., 2017), particularly with respect to the fundamental issue of fast, unobservable nonstationarities in background dynamics.

## 2 Results

To empirically motivate the characteristics of monosynaptic spike interactions *in vivo*, we begin by analyzing a large dataset that partially deconfounds monosynaptic effects from background network activity through juxtacellular perturbation of excitatory neurons in the hippocampus of awake mice (English et al., 2017). This study focuses primarily on pyramidal cell (PYR) to interneuron (INT) subcircuits in CA1. The persistence of finely-timed INT spikes following experimentally-evoked PYR spikes is strongly suggestive of the existence of a monosynaptic connection (Figure 1A) and, correspondingly, confirms previous interpretations in spontaneous data (Csicsvari et al., 1998; Fujisawa et al., 2008). We used ground truth labels reported by the experimentalists, which were only based on segments of the recording where the PYR was being juxtacellularly stimulated. Then, we decomposed the cross-correlograms of spontaneous spiking using multiple-comparisons-corrected interval jitter hypothesis tests (Amarasingham et al., 2012). These procedures test the null hypothesis that, conditioned on a coarsening of the INT spikes at timescale  $\Delta$  and on the PYR spikes, the conditional probability on INT spike timing is uniform (so-called “conditional uniformity”; this formulation is developed in greater detail below, see Methods). To isolate excursions from independence at each timescale, the proportion and number of bins of the CCG exceeding simultaneous acceptance bands were computed (Figure 1B). Simultaneous acceptance bands provide multiple comparisons corrections by controlling the global likelihood of false rejection at *any* lag, so that no particular lag of an interaction is assumed *a priori* (see Methods), an assumption that has been made in previous work. ROC analysis suggests an optimal timescale separation of  $\Delta = 17.3$ , for these test statistics as well as the labeling method of English and colleagues. Monosynaptic pairs are characterized by a short-latency peak in the causal direction of the CCG. At the  $\Delta$  yielding maximum AUC, the short-latency peak exceeding the detection threshold for synaptic pairs had an average width of 0.7521 ms and constituted on average 9.92% of the whole CCG (Figure 1C). These results indicate that monosynapses identified in English et al. 2017 can be identified in spontaneous data by timescale decomposition and that optimal detection is achieved through analysis of *sub*-millisecond dynamics.

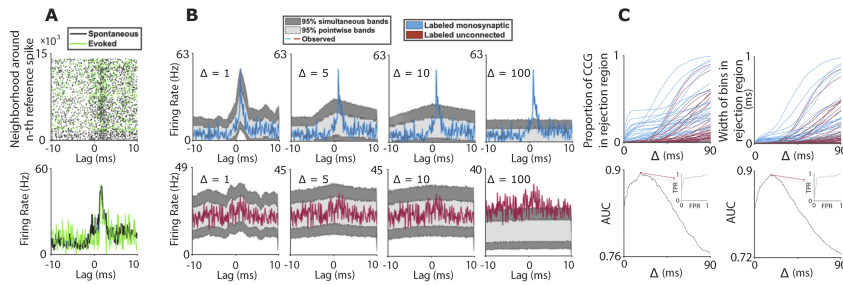


**Fig 1 Fine timescale interactions from *in vivo* data.** **A:** A putative monosynaptic pair. Top panel: Each row corresponds with the occurrence of a spike of one putatively presynaptic pyramidal neuron. The dots plotted across a row represent spike times of a (putatively post-synaptic) interneuron relative to the pyramidal neuron spike, which occurs at lag 0. Note that in this scheme the same interneuron spike may be represented in multiple rows. Green points represent interneuron spikes occurring within -10 to 10 ms of pyramidal spikes that fire during a juxtacellular stimulation period ('evoked' state), while black points are local to pyramidal spikes ('spontaneous' state), in the absence of stimulation. Bottom panel of A: Cross-correlograms for the same pair in top panel, each normalized by the number of pyramidal spikes. The reference train is the pyramidal neuron. Though the evoked pyramidal spikes occur during stimulation, there is still an over-abundance of finely-timed spikes in the interneuron shortly after pyramidal spikes, providing evidence for a monosynaptic connection. **B:** Quantifying the evidence for fine temporal structure in cross-correlograms. The top panels show the spontaneous CCG of a neuron pair labeled monosynaptic and bottom panels for a pair labeled unconnected. The gray bands are acceptance bands for jitter hypothesis tests (see Methods).  $\Delta$ 's on the plot are in units of milliseconds. **C:** For each examined spike train pair, the proportion of the cross-correlogram that exceeds (rejects) simultaneous acceptance bands is plotted for a range of  $\Delta$  (top left panel). Each line corresponds with a spike train pair labeled by the methods of English et al., 2017 as either monosynaptic (blue lines), or unconnected (red lines). Additionally, the number of bins (in units of ms) that exceed the simultaneous acceptance bands in the CCG is used for the same analysis (top right panel). Each test statistic is used as a classifier, and the AUC (area under the ROC curve for that classifier) relative to the ground truth labels is plotted as a function of  $\Delta$  (adjacent bottom panels).

In the following section, we develop the simplest biophysical models possible that can account for the individual and pairwise spiking dynamics described above. First, we describe an integrate-and-fire neuron driven by a stochastic input characterized by fast-timescale nonstationarities. A pair of such integrate-and-fire neurons are coupled by common, rapid fluctuations in the statistical parameters governing the stochastic input terms for each neuron. These noisy input processes model the neuron's background input, decoupled from any monosynaptic connections. We then model a monosynaptic connection between the two neurons in two steps. In the first step, we explicitly induce a spike in the postsynaptic neuron a few milliseconds after randomly-chosen spikes in the presynaptic neuron ('injected synchrony'). In the final step, we substitute this injection process with a conductance-based model of the monosynapse. We pose the statistical challenge, in this setting, as that of inferring the modeled monosynaptic properties directly from spike timing observations. We develop inference methods from the injected synchrony point of view. The challenge is to do so in the setting where the nonstationarities driving the background input terms are rapid enough that the direct inference of their underlying statistical parameters would be challenging. To examine this challenging regime, we circumscribe the problem somewhat by making explicit modeling choices. We will defer the discussion of alternative choices, and related issues of interpretation, to the Discussion. We will expand on these issues in the course of developing the biophysical and statistical models.

## 2.1 Biophysical Models

Integrate-and-fire neurons offer a minimal set of mathematically tractable equations that remain faithful to cellular physiology (Gerstner et al., 2014). They are among the most common models in theoretical neuroscience, and their performance at predicting spike times at millisecond precision has been demonstrated in multiple studies (see Gerstner and Naud (Gerstner and Naud, 2009) for review). Thus they are natural candidates for reproducing spike time-based *in vivo* observations. We constructed these models under the constraint that they quantitatively reproduce the spike auto- and cross-correlograms reported in *in vivo* studies, and that their parameters are physiologically plausible (see Methods).

The basis of our biophysical modeling is a noise-driven leaky integrate-and-fire neuron with a fast adaptive threshold. Two variables characterize the dynamical state of such a neuron: the membrane potential  $V$  and the voltage threshold  $V_T$ . A spike is emitted whenever  $V$  positively crosses  $V_T$ , which in turn forces  $V$  to be reset instantaneously to a fixed value. The dynamics of these two variables are controlled by deterministic equations. While the membrane potential  $V(t)$  is constrained by a passive membrane model and the input  $I(t)$ ,

$$\tau_m \frac{dV}{dt} = -V + I. \quad (1)$$

the threshold  $V_T(t)$  is constrained by a sodium channel model and  $V(t)$ ,

$$\tau_T \frac{dV_T}{dt} = -V_T + f(V), \quad (2)$$

$f$  being a linear rectifier function. The input  $I(t)$  is a stochastic process and is intended to mimic the background network activity as seen from the site of spike initiation (see Discussion),

$$\tau_I \frac{dI}{dt} = -I + \mu + \sigma \sqrt{\frac{\tau_I}{2}} \xi, \quad (3)$$

with  $\xi$  a Gaussian white noise of zero mean and unit variance. (As will be apparent later, this background will explicitly exclude the monosynaptic connection between neurons when two integrate-and-fire neurons are modeled as a monosynaptic pair.) Details of the biophysical equations can be found in the Methods.

### 2.1.1 Nonstationary firing

In principle, a neuron's firing rate at time  $t$  refers to the instantaneous probability of spiking for specified experimental conditions. This notion is subjective, as it presumably depends on the point of view of an observer with limited information. (For this reason, what we typically refer to as 'nonstationary' firing in experimental contexts, is in fact model misspecification, from the point of view of statistics; Harrison et al. (2013); Amarasingham et al. (2015).) Our theoretical perspective in this study is largely that of nonparametric statistics. In contrast to the typical experimental situation, here we work with an explicit model for the biophysical dynamics, so we can specify explicitly that the spike train's probabilistic structure derives from lack of knowledge about the input  $I(t)$ , which models the background. As a consequence, in the rudimentary setting described above, the model has rich dynamical and statistical structure, but the 'firing rate' does not evolve over time (or repeat across 'trials'; indeed, there is no trial structure), because the drift term  $\mu$  is time-invariant (Aviel and Gerstner, 2006; Gerstner, 2000; Ostojic, 2011; Gerstner et al., 2014).

To give ‘nonstationarity’ an explicit meaning, let us consider the setting where  $\mu(t)$  is itself a rapidly-varying stochastic process, as a model of *in vivo* trial-to-trial variability. That is, in the context of this particular model, we are interested in studying the regime where  $\mu(t)$ , which is taken as unknown, varies quickly enough to challenge standard averaging approaches (such as derived from maximum likelihood) to neurostatistical inference. Here the inference of interest is of monosynaptic properties. Such a model is in the spirit of ‘doubly-stochastic’ spiking models (Churchland and Abbott, 2012) (but, again, see Amarasingham et al. (2015) for some warnings about this language).<sup>1</sup> A natural choice in this direction is to introduce a stochastic  $\mu(t)$  that varies on a slower timescale than the Gaussian colored noise. Formally, motivated by simplicity, we model  $\mu(t)$  as piecewise constant on equal-length intervals with random independently- and uniformly-distributed amplitudes (see Figure 2A),

$$\mu(t) = \sum_{i=1}^m \mu_i \mathbb{1}\{(i-1)D_\mu \leq t < iD_\mu\}, \quad (4)$$

where  $\mathbb{1}\{A\}$  represents the indicator function of  $A$  (i.e., taking the value 1 when the expression  $A$  is true, and 0 otherwise). The length of the intervals,  $D_\mu$ , models the timescale of this source of spiking variability.  $\mu_1, \mu_2, \dots, \mu_m$  are independent and uniformly-distributed (see Methods for details). For now, we view a realization of  $\mu(t)$  as an *approximation* to a smooth function. The motivation for this form of approximation is related to details of the statistical tools we will use (e.g., ‘interval jitter’ and related tools, to be described below) for inference, and will simplify the biophysical-statistical correspondence we seek to examine. Later, we will relax this assumption and find that our principal conclusions are robust to the piecewise constant form, using noise processes  $\mu(t)$  with continuous realizations.

We simulated this integrate-and-fire neuron numerically (see Methods). Spike auto-correlograms (ACG’s) computed from the generated spike trains are shown in Figure 2A, using two sets of parameters. The parameters were tuned so that the ACG’s qualitatively resemble those observed *in vivo* in hippocampal pyramidal cells and interneurons (Barthó et al., 2004; English et al., 2017; Sirota et al., 2008; Quilichini et al., 2010), under the constraint that biophysical parameters remain within physiologically-plausible ranges.

We measured the firing statistics for the two model cells in our simulations and observed: a mean firing rate of 1.6 Hz and a CV of 1.04 for the pyramidal cell; a mean firing rate of 21.6 Hz and a CV of 0.91 for the interneuron.

### 2.1.2 Co-modulated firing

Thus far we have described biophysical models of single neuron dynamics, but microcircuit connectivity inference involves the analysis of at least a pair of spike trains. Two neurons that are not monosynaptically connected can emit spikes that appear correlated on a millisecond-timescale even if the underlying coupling mechanism operates on a slower timescale (Brody, 1999; Ventura et al., 2005; Yu and Ferster, 2013). We proposed a simple mechanism of firing co-modulation. The circuit is composed of two integrate-and-fire neurons, as just described, but the piecewise constant input is now common to both neurons (exactly the same in both neurons). The two Gaussian colored noise processes remain independent. We simulated this microcircuit numerically (CCG in Figure 2B). Here we use the same parameters we used previously for reproducing a pyramidal and an interneuron ACG’s. The CCG exhibits a hump-shaped envelope typical of slow co-modulation.

<sup>1</sup> To be explicit about the subtlety in the setting here: in fact, we will model  $E[\mu(t)]$  as time-invariant (Eq. 4). Thus, for an observer that does not know  $\mu(t)$ , the spike probabilities are time-invariant. On the other hand, for an observer that knows  $\mu(t)$ , the spike probabilities are not time-invariant.

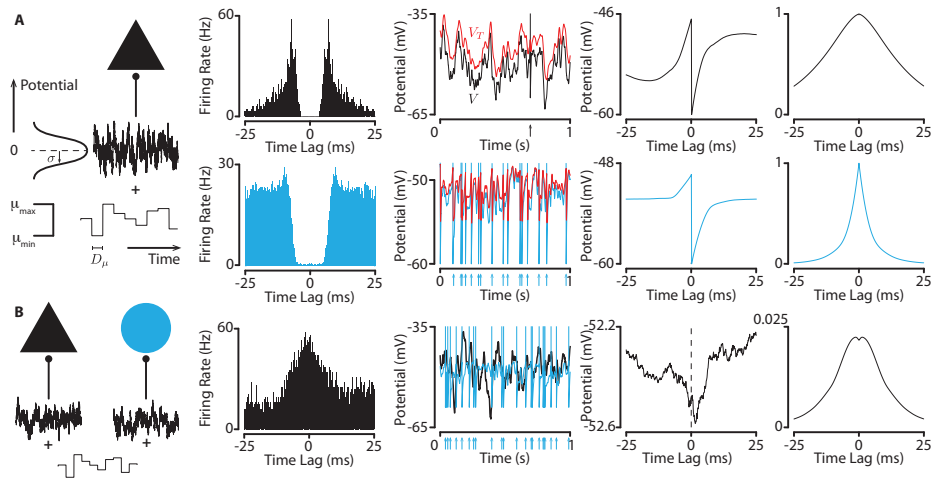


**Fig 2 Biophysical models of background firing.** **A:** Model of nonstationary firing based on a single neuron. The neuron is a standard leaky integrate-and-fire (membrane time constant: 10 ms), but with a fast adaptive threshold (threshold time constant: 1 ms, for the interneuron model). Its input is the addition of a fast Gaussian colored noise (auto-correlation time constant: 10 ms) and a slow piecewise constant function of uniformly random amplitude (fixed interval length: 10 ms). Model parameters were tuned so that the resulting spike auto-correlogram resembled either the auto-correlogram of a hippocampal CA1 pyramidal neuron (top panels, in black), or of a CA1 interneuron (bottom panels, in blue). **B:** Model of co-modulated firing based on a pair of pyramidal cell (black triangle) and interneuron (blue disk). The parameters of each cell's model are tuned exactly as in A. For each model, we represent (left to right): the spike auto-/cross-correlogram; the underlying membrane potential traces (black for pyramidal and blue for interneuron) with the associated dynamical spike threshold (red; a spike time is indicated with an arrow); the spike triggered average of the membrane potential; the auto-/cross-correlation function of the membrane potential. In the pairwise model, the pyramidal spikes are taken as reference.

*Ultra-precise monosynaptic spike transmission from artificially injected spikes* First we implemented an artificial mechanism of ultra-precise synaptic spike transmission, on the basis of the microcircuit just described. The pyramidal model is taken as presynaptic, and the interneuron model as postsynaptic. For each randomly chosen presynaptic spike, we created a postsynaptic spike delayed by a given latency. We call the created spike pair “injected synchrony.” Although this model is not purely biophysical, it has the advantage of allowing the control of the number of synaptically transmitted spikes, independently of the background input. An example of a CCG resulting from such a model, can be seen in Figure 3A.

### 2.1.3 Ultra-precise monosynaptic spike transmission from input conductance dynamics

Our most complete biophysical model of a monosynaptically connected cell pair is based on the co-modulated firing mechanism, but the target neuron receives an additional input. This input is classically described as an input current  $g_s(E_s - V)$  to the membrane equation (Eq. 1), where  $g_s$  is the synaptic conductance, and  $E_s$  is the synaptic reversal potential. More precisely, each presynaptic spike increments  $g_s$  by a fixed amount, following a fixed latency delay, which then decays exponentially to its baseline level,

$$\tau_s \frac{dg_s}{dt} = -g_s. \quad (5)$$

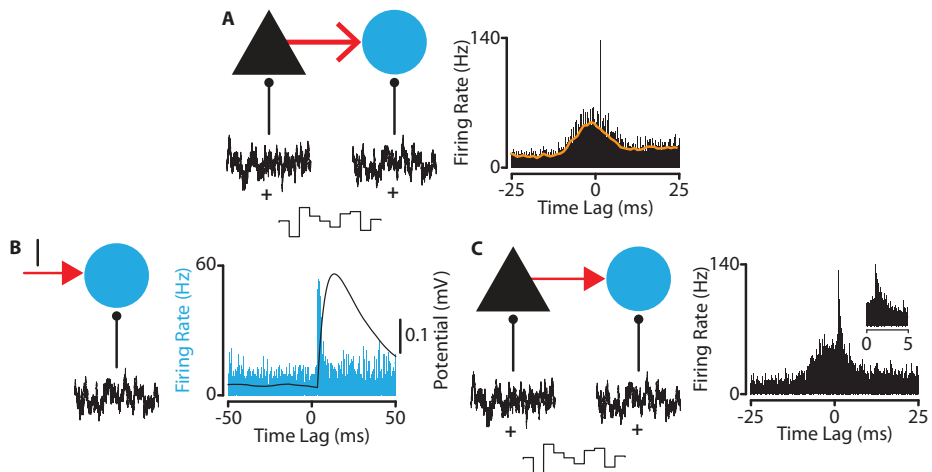


**Fig 3 Biophysical models of ultra-precise monosynaptic spike transmission.** **A:** In the basic model, the monosynaptically transmitted spikes were artificially added to the target train, by delaying a random subset of reference spikes with short latency. This resulted in the black cross-correlogram. The superposed orange line indicates the smoothed envelope of the cross-correlogram associated with the same model without synapse. **B-C:** In the more realistic model, a synapse is modeled as a dynamic input conductance triggered by presynaptic spikes. **B:** We considered first a single interneuron model, whose synaptic input conductance was triggered by a single spike in each trial. The spike count was averaged over trials, and normalized to be homogeneous to a firing rate - poststimulus time histogram. The postsynaptic membrane potential was measured relative to the presynaptic spike time, and then averaged over trials (black line) - spike-triggered average. Note the sharpness of the poststimulus time histogram in comparison to the spike-triggered average. **C:** The synapse was then incorporated into the firing co-modulation circuit. The interneuron's synaptic input conductance is triggered by the pyramidal cell's spikes. The cross-correlogram between the pre- and postsynaptic spike trains exhibits a sharp peak at short latency, similar to the *in vivo* observations.

As a result, the dynamics of  $g_s(E_s - V)$  following a single presynaptic spike mimics the typical trajectory of a postsynaptic current (PSC). See Methods for more details.

First, we simulated solely our interneuron model with such synaptic input dynamics, and emitted a single presynaptic spike in each trial. This simulation allows the study of synaptic spike transfer irrespective of the presynaptic spike train's temporal and statistical structure. We repeated the simulation over many trials (10,000), counted spikes in each elementary time bin (0.1ms) for every trial, and averaged the normalized count over all trials – this creates a poststimulus time histogram (PSTH) as shown in Figure 3B. Similarly, we measured the membrane potential at each time bin and averaged it over trials – this creates a spike-triggered average (STA) (see Fig. 3B). We note that the resulting PSTH peak is extremely sharp (half-width < 2.5ms), while the STA decays smoothly. The transformation of a standard postsynaptic potential (PSP) into a fast firing response has been previously explained by several authors (see Discussion), and can be mostly attributed here to the low variability of the Gaussian colored noise. The transition from sharp (half-width 2.5 – 10 ms) to extremely sharp (half-width < 2.5ms) PSTH can be accounted for by the fast adaptive threshold and its short time constant (see Fig. 3B). Second, we simulated the full synapse model over a single long trial (5,000 s), taking the pyramidal model as presynaptic and the interneuron one as postsynaptic, and showed the resulting CCG in Figure 3C. We still observed in this more complete setup the extreme sharpness of spike time correlation, despite the complexity of the presynaptic spike train, which highlights the robustness of the effect.

Note that the PSP amplitude that gave rise to the CCG peak is not strong in our experiment (PSP  $\approx 0.35$  mV in the absence of background noise).

## 2.2 Estimating Excess Synchrony: Separation of Timescale and Injected Synchrony

We have presented the various biophysical models used for generating spike data that reproduces typical *in vivo* firing statistics (i.e., ACG's and CCG's). In what follows, this data will be taken as ground truth for studying the statistical problem of monosynaptic inference in nonstationary conditions. For this purpose, we develop a statistical model for a monosynaptically-connected pair of spike trains that dissociates postsynaptic spike train structure into coarse and fine timescale components. The fine timescale component is associated with monosynaptic phenomena, and induces fine-timescale correlations between the pre- and postsynaptic spike trains. The coarse timescale component effectively models the influence of unobserved synaptic inputs (the ‘background’), and is designed in mind of the concern that the background process is confounded by nonstationary effects.

### 2.2.1 Formulation

The postsynaptic train is modeled as a superposition of two trains: a *background* spike train ( $\mathbf{B}$ ) and an *injected* spike train ( $\mathbf{I}$ ). The statistical properties of the background train are modeled nonparametrically to accommodate nonstationarity. Technically, the nonparametric model is that the conditional probability distribution on the background spike train is uniform, conditioned on knowledge of the reference train and on knowledge of the spike counts of the target train in intervals of length  $\Delta$ .  $\Delta$  parameterizes the characteristic timescale of the background spike trains. We make this precise as follows.

A spike train,  $\mathbf{R}$  for example, is modeled in discrete time, and we write  $\mathbf{R} = (R_1, \dots, R_{|\mathbf{R}|})$ , where  $R_i$  is the time of the  $i^{\text{th}}$  spike in  $\mathbf{R}$ , and  $|\mathbf{R}|$  is the number of elements in  $\mathbf{R}$ . Time is partitioned into equal-length intervals of size  $\Delta$ , and the spike counts in  $\mathbf{R}$  in the intervals are denoted  $\mathbf{N}(\mathbf{R}) = (N_1(\mathbf{R}), \dots, N_m(\mathbf{R}))$  where  $m$  is the number of intervals (Amarasingham et al., 2012).

The time discretization specifies the resolution of synchrony. Here the trains  $\mathbf{R}$  and  $\mathbf{T}$  will be referred to as the reference and target, respectively. In addition, we impose the condition that all intervals that contain a spike in  $\mathbf{T}$  also contain a spike in  $\mathbf{R}$ . (Spikes in the target train that do not satisfy this condition are not in  $\mathbf{T}$ .)

Given  $\mathbf{R}$  and  $\mathbf{T}$ , their synchrony count is defined as,  $S = \sum_{i=1}^{|\mathbf{R}|} \sum_{j=1}^{|\mathbf{T}|} \mathbb{1}\{T_j - R_i = \text{lag}\}$  where lag  $> 0$  represents the synaptic delay in units of time bins.

### 2.2.2 Injected Synchrony Model

When evaluating a cell pair that is putatively monosynaptic, the candidate presynaptic train is chosen as reference and the candidate postsynaptic train as target. In the following, we will assume that the reference train is fixed and the target train is random. (Technically, the probability distribution on  $\mathbf{T}$  is in fact the conditional probability distribution on  $\mathbf{T}$ , given  $\mathbf{R}$ .) The model (“injected synchrony”) is that (conditioned on  $\mathbf{R}$ ), the target train  $\mathbf{T}$  is a superposition of two point processes: an “injected” train,  $\mathbf{I}$ , and a “background” train,  $\mathbf{B}$ .  $\mathbf{B}$  is assumed to be conditionally uniform, conditioned on  $\mathbf{N}(\mathbf{B})$  and  $\mathbf{R}$ . In other words, conditioned

on  $\mathbf{N}(\mathbf{B})$  and  $\mathbf{R}$ , all spike trains  $\mathbf{B}$  (that are consistent with  $\mathbf{N}(\mathbf{B})$  and  $\mathbf{R}$ ) are equally likely.<sup>2</sup>  $\mathbf{T} = \mathbf{B} + \mathbf{I}$ , where  $+$  denotes superposition (of point processes). Note that two spikes can be in the same bin in the superposition, which is an approximation. All of the spikes in  $\mathbf{I}$ , on the other hand, are assumed to be synchronous with  $\mathbf{R}$ . The synchrony is delayed by the parameter lag, meaning that all spikes in  $\mathbf{I}$  occur lag time bins after a spike in  $\mathbf{R}$ .<sup>3</sup> Given the model, the inference problem is to estimate the number of ‘injected’ synchronies,  $\theta = |\mathbf{I}|$ .  $\theta$  and  $\mathbf{R}$  are fixed, and, for now, we assume that the background timescale  $\Delta$  is known. In effect, the inference problem asks: what is the excess synchrony, assuming there is a background process that has time scale  $\Delta$ ?

The model induces a decomposition of the total synchrony,  $S$  as

$$S = S_\Delta + \theta, \quad (6)$$

where the synchrony count  $S_\Delta$  are synchronous pairs composed of background spikes (sometimes called chance or accidental synchrony), and the synchrony count  $\theta$  is the number of injected spikes (sometimes called excess synchrony) [see Methods].  $S_\Delta$  and  $\theta$  are latent (unobserved) random variables.

Thinking in terms of neurophysiology, the essence of this model is the assumption that a spike (in the target train) can be unambiguously labeled as caused by *either* a slow (background) process, *or* a fast synchrony-inducing process. The statistical problem is to separate the fast synchrony ( $\theta$ ) from the slow synchrony ( $S_\Delta$ ) without access to the labels. The timescales of fast and slow are quantitatively modeled through the characteristic timescale  $\Delta$ . Correspondingly, the model breaks down when such a causal attribution is ambiguous (and would likely require, among other components, a multiscale framework), as for example, in the case of weak synapses (see Discussion). This is the sense in which the model expresses a ‘separation of timescales’ hypothesis for monosynaptic characterization.

The injection model in the case  $\theta = 0$  is in fact the null hypothesis for the *interval jitter* hypothesis testing procedures successively elaborated in precursor work (Amarasingham et al., 2012; Date et al., 1998; Platkiewicz et al., 2017). Statisticians commonly advise that tests of hypotheses be accompanied by an assessment of magnitude of effect, to distinguish ‘scientific’ significance from ‘practical’ significance, among other motivations (Wasserman, 2013). Injected synchrony can be motivated as one such measure for interval jitter hypothesis tests. This motivation has other applications in neurophysiology (see Martin and von der Heydt (2015); Shahidi et al. (2019) for precise examples).

### 2.2.3 Point Estimation

Consider a spike train pair generated by the injected synchrony model. An implication of the conditional uniformity assumption for a spike train  $\mathbf{B}$  is that one can randomly translate the spikes in  $\mathbf{B}$  without changing its statistical properties, so long as one preserves  $\mathbf{N}(\mathbf{B})$ , the spike counts in the intervals. This is one basis for the interval jitter hypothesis tests referred to above. In practice, this can be done by Monte Carlo sampling from the uniform distribution on the set of spike trains consistent with  $\mathbf{N}(\mathbf{B})$ . When used to generate surrogate

<sup>2</sup> No constraints are placed on the probability distribution of  $\mathbf{N}(\mathbf{B})$  itself, and this is the source of robustness to nonstationarity, broadly defined. This conditional modeling framework for modeling temporal structure in spike trains is motivated and developed from several points of view in prior work (Amarasingham et al., 2012, 2015; Harrison et al., 2015, 2013).

<sup>3</sup> For intuition, a canonical example can be constructed by generating two distinct independent, background spike trains, and superposing a homogeneous Bernoulli process synchronously (with appropriate lag) onto both trains (see Amarasingham et al. (2012), for example, for examples based on Cox processes for the background.)

data for hypothesis tests, this procedure is called *interval jitter*, because the original spikes in  $\mathbf{B}$  are, effectively, *jittered* (noting that these jitter perturbations are distorted slightly via the role of the interval positions, and also that such tests can also be performed analytically). In correspondence to this computation, a natural, naive estimate of the amount of injected synchrony  $\theta$  would consist in jittering all the spikes, computing the resulting synchrony, and subtracting it from the original (observed) synchrony. Variations of this “jitter-corrected” synchrony estimate have been implemented in the literature, although described in less formal terms (Amarasingham et al., 2012; Martin and von der Heydt, 2015; Smith and Kohn, 2008; Fujisawa et al., 2008). Informally, the mean of the resulting jitter-derived distribution furnishes an estimate of  $\theta$ , and, speaking loosely again, the spread of that distribution would provide some measure of variability. However, it is not hard to see, as clarified by the timescale model here, that this would introduce bias into the estimate, since the logic of jitter resampling only applies to the background spikes. Presumably, a more appropriate procedure would jitter only the spikes in  $\mathbf{B}$ . But, without access to the labels identifying  $\mathbf{B}$  and  $\mathbf{I}$ , it is not possible to distinguish an injected spike from a background spike. The naively-resampled injected spikes would contribute to the synchrony counts in the jitter-derived distribution only, thus corrupting the estimate of  $\theta$ .

A more refined approach consists in incorporating a probability distribution on these labels. We make an assumption that, given knowledge of the reference train and  $\theta$ , all consistent labelings of the target train are equally likely (all labels are equally likely, ‘LEL’). This includes as a special case the situation where the injected process is statistically homogeneous (in time) and independent of the background process, though the model is more general.

Then define

$$\bar{r} := \frac{1}{|\mathbf{T}|} \sum_{i=1}^{|\mathbf{T}|} N_{r,i}, \quad (7)$$

where  $N_{r,i}$  specifies the number of spikes in the reference train in the interval containing the  $i$ ’th target spike, and  $|\mathbf{T}|$  is the number of spikes in the target train. In the Methods section, we show that it then follows that, under the LEL assumption,

$$\hat{\theta}_{LEL} = \frac{S - \frac{\bar{r}}{\Delta} |\mathbf{T}|}{1 - \frac{\bar{r}}{\Delta}} \quad (8)$$

is an unbiased estimator of  $\theta$ :

$$E[\hat{\theta}_{LEL}] = \theta. \quad (9)$$

Notably, in the specific case that the number of spikes in the reference train is constant in non-empty intervals, unbiasedness holds independently of the LEL assumption; the latter situation is particularly relevant in the case of sparse firing (where sparseness is defined relative to  $\Delta$ ). The formula emphasizes the role of  $\Delta$  in the estimation of  $\theta$ .

#### 2.2.4 Validating the theoretical predictions

To validate our proposed formula (Eq. 8), we used the biophysical model with monosynaptically injected spikes. First, we simulated numerous trials with this model (1,000 trials of 1,000 s duration), injecting the same amount of synaptic spikes in each trial ( $\approx 110$  spikes; about half of the total synchrony count). We estimated for each trial the amount of excess synchrony using both our formula and the standard jitter-corrected subtraction. In the formula, we used for the jitter interval length ( $\Delta$ ) the interval duration of the piecewise constant input ( $D_\mu$ ). We represented the empirical distribution for both estimates in Figure 4A. One can

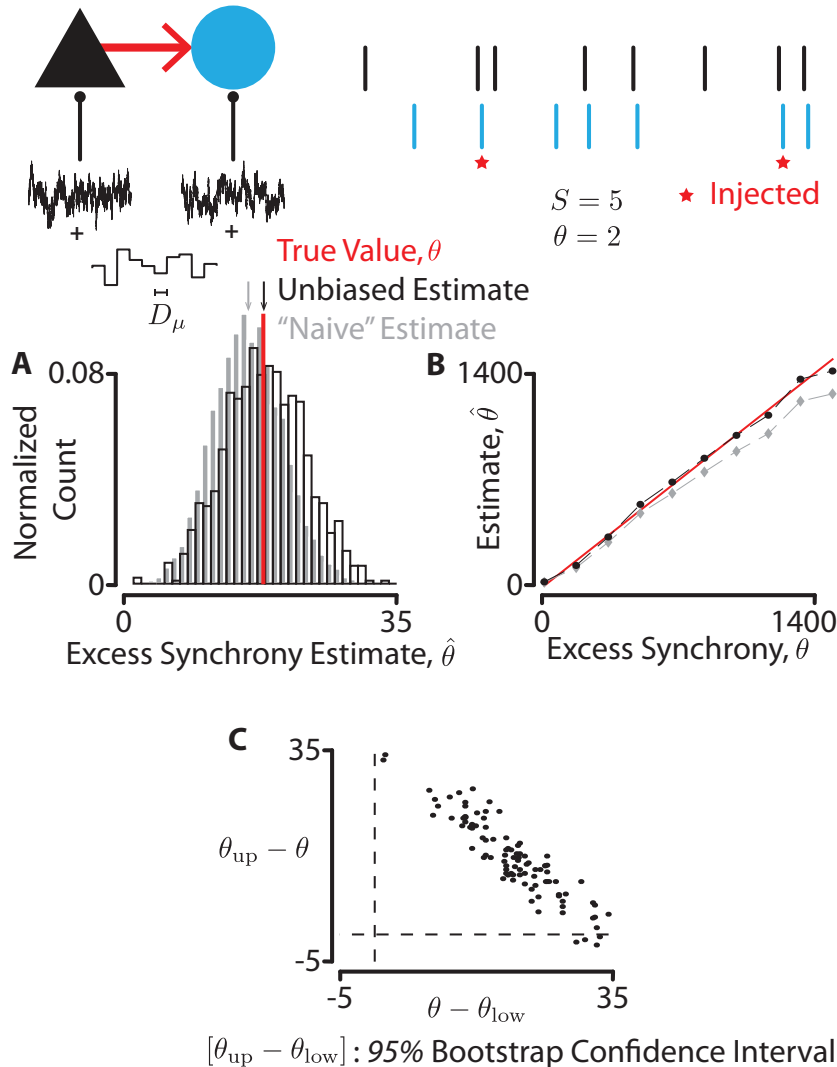


**Fig 4 Estimation of the excess synchrony.** In these numerical experiments, we implemented only the synapse model with artificial spike injection. **A:** In this numerical experiment, we generated multiple spike train pairs using the biophysical model (1,000 trials of 1,000 s duration), but kept the number of injected spikes the same across trials (solid red line;  $\approx 110$  spikes). We estimated the amount of injected spikes for each trial using both our closed-form formula (black), and a subtraction of the jitter-corrected synchrony count from the total synchrony count (gray), taking the jittering interval length equal to the piecewise constant input's interval length. The arrows in the corresponding colors indicate the average of each distribution. Note that the closed-form estimate is closer to the true value compared to the standard jitter-corrected estimate. **B:** Similar numerical experiment (10 trials of 10,000 s), analysis, and color code, but the amount of injected spikes was varied across trials. The solid black line indicates the first diagonal. Note that the discrepancy between the naive estimate and the true count increases with the true count, while it remains the same for our proposed unbiased estimate. **C:** Similar numerical experiment to the one performed in A (100 trials of 1,000 s). We computed the lower and upper bounds of the 95% bootstrap confidence interval for each trial, taking the jittering interval length equal to the piecewise constant input's one. In 95% of the trials, the true injected synchrony count fell into the confidence interval.

check that the distribution of the unbiased estimate is centered around the true injected count, unlike the standard jitter-corrected estimate. Additionally, the unbiased estimate's average is closer to the true value than the naive estimate's average. This numerical experiment confirms the relevance and the accuracy of the theoretical prediction for the injected count estimate. It also confirms that the statistical injected synchrony model can plausibly be mapped onto an integrate-and-fire neural circuit – the background firing produced by the LIF-based model is well captured by the jitter null here. Second, we replicated the experiment (10 trials of 10,000 s duration), but injected a different number of synaptic spikes in each trial (ranging from 0 to 1,000 spikes in increments of approximately 100). For each trial, we computed the unbiased and naive estimates, as shown in Figure 4B. The results confirm the observations made in the previous experiment. It also shows that the unbiased estimate is close to the true value for sufficiently long trials (the trials are 10 times longer than in the previous experiment), and that the bias of the naive estimate increases as the true value increases. The last observation can be understood by recalling that all the spikes are jittered in naive estimation, including the injected spikes.

### 2.2.5 Bootstrap Interval Estimation

While a formula for a point estimate of the synaptically injected count is appealing, we have seen in our numerical experiments that  $\hat{\theta}$  can vary substantially around  $\theta$ , especially for highly nonstationary firing and short time windows. This motivates construction of a bootstrap confidence interval to assess this variability. (In the Appendix, we sketch the construction of more general, and exact, confidence intervals through direct application of conditional inference ideas, but we do not here pursue this idea numerically.) Here we propose a simple method for deriving such an interval based on our closed-form estimate (see Methods). The principle consists in computing numerous estimates of  $\theta$  using Eq. 8, based on spike trains generated (via bootstrap resampling of the background spikes) under the injected synchrony model. One can then derive an  $\alpha$ -level confidence interval from the resulting empirical distribution of the estimates, by peeling off lower and upper percentiles. The problem with such a resampling scheme is that we do not know which spikes were injected, and how many injected spikes there are. One way to circumvent this is to assume that the injected spikes were uniformly distributed among the target spikes (LEL), and to substitute  $\hat{\theta}_{LEL}$  for the number of injected spikes. We validated this technique by simulating the previous biophysical model. We ran the simulation over numerous trials (100 trials of 1,000 s duration), and injected in each trial the same number of synaptic spikes. We computed the bounds of the 95% bootstrap confidence interval for each trial, and counted the number of times the true value lied in the interval (see Fig. 4C). In 95% of the trials the true value was trapped by the interval.

### 2.2.6 Estimating a Monosynaptic Peak Conductance From Spikes

We validated our statistical predictions on the data generated by our biophysical model with monosynaptically injected spikes. This suggests that spike trains generated using integrate-and-fire models can fit in the jitter null. Additionally, the LIF models' parameters were tuned to give rise to ACG's and CCG's that look qualitatively similar to the ones observed *in vivo*, which is a strong indication that jitter is appropriate for *in vivo* spike data analysis. However, it is also important to test whether the equally likely labeling is a relevant assumption. In all of the previously discussed simulations, synaptic synchronies were artificially injected and thus satisfy the labeling (separation of timescales) assumption by construction. To address this

concern, we implemented the synaptic conductance model. We first conducted a simulation where the synaptic peak conductance,  $g_0$ , is time-independent but varies between trials (over 10 trials). We ensured that the trials were long enough (10,000 s) for the excess synchrony estimate  $\hat{\theta}$  to approach its average value. We computed  $\hat{\theta}$  for each trial using Equation 8, choosing a resampling interval length of the piecewise constant input's timescale and taking a synchrony window of size 5 ms (this last value was numerically tuned to provide the largest synchrony count). We measured for each trial the “true” injected synchrony count,  $\theta$ , by replicating the trial with the same exact instantiation of noise but “turning off” the synapse ( $g_0 = 0$ ), and computing the difference in synchrony between the original and the replicate. We first checked that our estimate  $\hat{\theta}$  was linearly correlated with  $\theta$  ( $R = 0.99$ ,  $p = 1.53 \times 10^{-10}$ ), as can be seen in Fig. 5A. This result confirms that our theoretical prediction extends to a situation that is more biophysically realistic. In particular, it gives support to the equally likely labeling assumption. Second, we checked that  $\hat{\theta}$  was monotonically related to  $g_0$ , as can be observed in Figure 5A. In this experiment the correlation is almost linear, but we do not expect it to generalize to larger synaptic conductance ranges, as highlighted in Rossant et al. (2011). In a second simulation, we allowed the synaptic peak conductance to vary along a trial in a stepwise fashion, using the same biophysical model. We analyzed a single trial, and computed  $\hat{\theta}$  in a sliding window of width  $10^5$  ms (a tenth of the whole trial duration). We converted the estimated value in equivalent PSP amplitude by applying a linear regression to the corresponding relationship obtained in the previous experiment (fixed peak synaptic conductance). The numerical result, shown in Fig. 5B, suggests that it is possible to dynamically track a transient connection strength, *in the sense of an order-preserving transformation*, despite a highly nonstationary firing background.

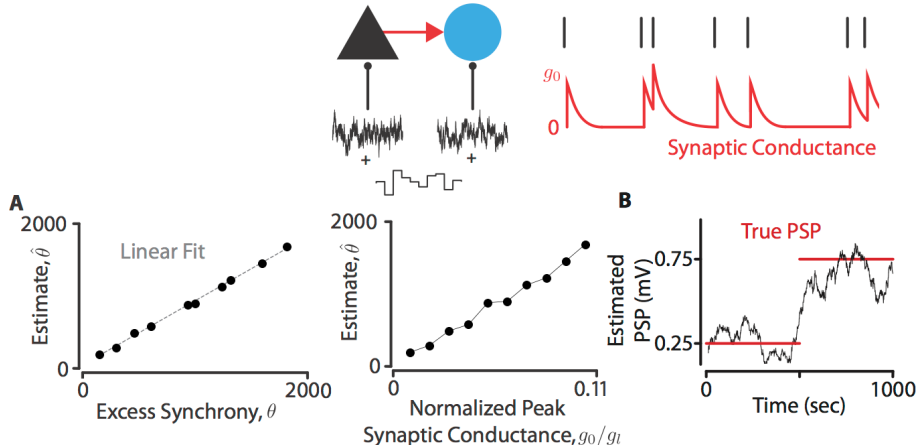


**Fig 5 Monosynaptic connection strength from spike times.** We implemented the synapse model with dynamic input conductance. **A:** The peak synaptic conductance value,  $g_0$ , was varied over trials, which induced a variation of the excess synchrony. (Left) The effect of this variation on the true excess synchrony,  $\theta$ , was measured by replicating the simulation using the same exact noise instantiation but removing the synaptic connection ( $g_0 = 0$  nS). The excess synchrony was estimated for each trial ( $\hat{\theta}$ ). The gray dashed line indicates the result of a linear regression. (Right) The solid black lines connecting the markers are simply here for illustration. **B:** The peak synaptic conductance value,  $g_0$ , was incremented at 500 s of a single 1,000 s trial. The value of the corresponding postsynaptic potential (PSP) peak is indicated (red). The estimate  $\hat{\theta}$  was computed in a sliding time window (with a width one-tenth of the whole trial duration). Its value (in equivalent units) is assigned to the center of each window.

### 2.2.7 Parametric Methods

Our method for detecting and quantifying connection strength is motivated by the point of view of nonparametric and (in the case of the injection model) semiparametric statistics. This method can be computationally expensive when it is necessary to generate a large number of surrogate trains (as in  $p$ -value computation), in addition to possibly introducing technical concepts and methods that are unfamiliar. A baseline alternative, implicit in much of the neurophysiology literature, is given by parametric statistics based on classical distributions (e.g., the spike train is generated by an inhomogeneous Poisson process), and in particular by parametric bootstrap methods (Amarasingham et al., 2012; Kass et al., 2014). A benefit of bootstrap in this setting can be that the null distribution of the test statistic can often be explicitly computed or at least quickly approximated, thanks to an explicit parametric model for the data (e.g., the Poisson model). Nevertheless, we will demonstrate here that, even in approximately Poisson spiking regimes, and essentially because of the timescales involved, the bootstrap test is a less sensitive synapse detector. Speaking to the broader issue of robustness to model specification, which we view as more fundamental, we provide a mathematical sketch in the Appendix demonstrating that the null hypothesis of conditional uniformity can essentially only be tested with a jitter method.

We simulated the biophysical model of firing co-modulation in the absence of synaptic connection. Here we tuned the parameters such that the firing of each LIF neuron is approximately Poisson (see Methods) (Stevens and Zador, 1996). More precisely, the spike trains are approximately inhomogeneous Poisson processes with an intensity function that follows the dynamics of the piecewise constant common input. We computed surrogate synchronies by generating numerous surrogate target trains (100 surrogates), and tabulating the amount of synchrony between the reference and each surrogate target train. In the jitter case, a surrogate train was generated by  $\Delta$ -jittering the original target spikes, with  $\Delta = D_\mu$  (the piecewise constant input's interval length). In the bootstrap case, a surrogate train was generated by first measuring the firing rate in each  $\Delta$ -interval, then generating spikes from a Poisson process whose intensity function is given by the measured firing rate (constant in each  $\Delta$ -interval, but that can vary between intervals.) (Note that the Poisson bootstrap can be computed analytically, although we do not do that here.) In a first numerical experiment, we generated numerous spike trains (1,000) of the same duration (500 s). In half of the trains, we injected the same number of spikes in each target train following our basic synaptic model (0, 5, 50, or 200 spikes). The fixed number of injected spikes ( $\theta$ ) was then varied across iterations of the experiment. (From a neurophysiological perspective, the simulated data can be seen as originating from a cell population of independent neuron pairs.) We declare that a synaptic connection is detected whenever the  $p$ -value is lower or equal than a given threshold. To compare the sensitivity of the two methods, we computed the  $p$ -values for both methods for a wide range of threshold values, and estimated for each threshold value (i.e., nominal false positive rate) the probability of synapse detection (i.e., true positive rate), by taking the ratio of detected synapses to total connected pairs. The result of our experiment is shown in Figure 6A. The verdict of the ROC is clear: here a jitter detector is more sensitive than a bootstrap, even in the Poisson regime in which the issue of model misspecification is presumed not to be an issue. This demonstrates the breakdown of bootstrap methods in highly nonstationary background firing regimes (Amarasingham et al., 2015), as we are reasoning that the background firing is approximately in the bootstrap null. (Note that the discrepancy is revealed by taking as the synchrony definition, the total target spike count in a 5 ms window centered around the CCG peak (Fujisawa et al., 2008; English et al., 2017). See the Supplementary Appendix for a quantitative explanation of the necessity of this.)

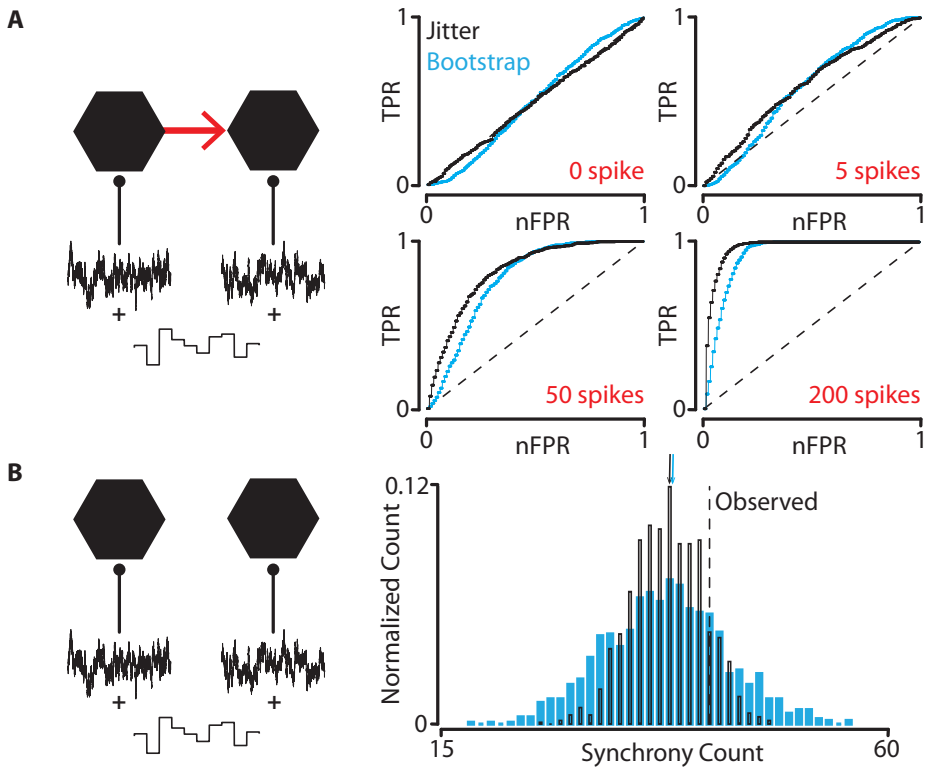


**Fig 6** Bootstrap vs. jitter synapse detector. **A:** (Left) A circuit composed of two monosynaptically connected standard LIF neurons was simulated over many trials (1,000 trials of 500 s duration). The neurons were driven by both two independent white noise inputs and a common piecewise constant random input. The white noise parameters were chosen so that their firing was almost Poisson (mean:  $V_T - 10$  mV with  $V_T$  the threshold; standard-deviation: 5 mV). The piecewise constant input was characterized by an interval length of 5 ms and an amplitude of 10 mV (i.e., maximum – minimum), making the Poisson firing highly inhomogeneous. The basic synapse model with spike injection was implemented. (Right) Modified ROC curves were computed based on the produced spike trains (nFPR: nominal false positive rate; TPR: true positive rate), for various amounts of injected synchrony (red). The  $p$ -values were computed using both jitter (black) and bootstrap (blue). The dashed line indicates the first diagonal. Note that all the jitter ROC curves lie above the bootstrap ones, confirming that the jitter has greater sensitivity of synapse detection. **B:** (Left) The connecting synapse was deleted from the circuit examined in A. (Right) For one simulation trial, a single synchrony count was observed (dashed line). Multiple surrogates ( $\approx 1,000$ ) were generated from the original target spike trains, both using a jitter (black edge) and a bootstrap (blue) resampling methods. The resulting synchrony empirical distributions are shown. Note the similarity of the means (indicated by the arrows), but the larger spread for the bootstrap.

The source of the difference in sensitivity can be intuited by looking at the distribution of surrogate synchronies for the two methods. We recall, indeed, that the  $p$ -value can be computed as follows,  $p = (1 + \sum_{j=0}^N \mathbb{1}\{S^{(j)} \geq S\})/(N+1)$ , where  $N$  is the number of surrogates,  $S$  is the total synchrony, and  $S^{(j)}$  is a surrogate synchrony ( $S^{(0)} = S$ , by convention). We took one pair of trains at random from the simulated ones without synapse. We computed numerous surrogate jitter and bootstrap synchronies (1,000 for each method), as described previously. One can observe that although both distributions are centered around the same average, the bootstrap synchrony distribution has a larger spread than the jitter synchrony one,

as shown in Figure 6B. Some calculations that clarify and explain these sensitivity effects mathematically are provided in the Appendix.

### 3 Discussion

The inference of microcircuit connectivity maps from *in vivo* recordings provides one of the important challenges in systems neuroscience. Such maps have been extracted in several studies (Fujisawa et al., 2008; Quilichini et al., 2010; English et al., 2017), but rely heavily on statistical, sometimes heuristic, techniques. The focus has been on the strongest functional synaptic connections. It is natural to aim at more subtle interactions, in particular regarding the detailed interactions between learning and synaptic plasticity (Dupret et al., 2013; Miyawaki and Diba, 2016; Watson et al., 2016), or the time course of weaker monosynaptic couplings, even in sparse firing conditions. With such ambitions in mind, we proposed a biophysical neuron model that reproduces two apparently paradoxical *in vivo* features: the sharp cross-correlogram peak at short-latency, and high interspike interval variability. We developed rigorous statistical models for extracting synaptic connection strength from fine-timescale spike pairwise correlations. We calibrated the physiological relevance of the statistical assumptions by applying it to spike data generated from the biophysical neuron model. We highlighted its potential for dynamically tracking minute synaptic changes, despite fast, non-trivial background fluctuations.

In parallel, from a more computational perspective, we illustrated a numerical mapping between a family of stochastic integrate-and-fire-type neurons driven by fast nonstationary noise and a semiparametric statistical model that accommodates the nonstationarities as nuisance parameters, which we referred to as the injected synchrony model. An additional benefit is a closed-form equation for estimating an effective synaptic strength parameter from spike data.

In the following, we discuss some alternative biophysical models. We propose physiological interpretations of the biophysical models. We point out some limitations of the injected synchrony model, and discuss how they might be resolved.

#### 3.1 Physiological Interpretation of the Biophysical Models

Our synapse model is based on the one proposed and examined by Ostojic et al. (2009). Of note, the extreme sharpness of the CCG peak, as found in physiological data, was not reproduced in this study. Furthermore, the authors cast doubt on the plausibility of this feature in the context of their model. We incorporated a few new components and tuned the parameters differently to recover these striking *in vivo* features. We detail here these modified elements along with their physiological meaning.

##### 3.1.1 Low Variability of Fast Noise

In our biophysical models, the ultra-precision of monosynaptic spike transmission relies critically on low variability of the fast input noise ( $\sigma \ll 10\text{mV}$ ). This hypothesis was first proposed and theoretically motivated by Herrmann and Gerstner (2001) in the context of motoneuron experiments (Herrmann and Gerstner, 2002). More precisely, the authors showed analytically that, in the low noise regime, the shape of the CCG peak is dominated by the positive part of the postsynaptic potential's time-derivative,  $d\text{PSP}^+/dt$ , making it extremely

sharp ( $d\text{PSP}/dt$  is only positive in the PSP's time-to-rise part). This fast noise input is supposed to capture the collective result of numerous weak synaptic dynamics driven by uncoordinated presynaptic spike trains. Here low noise means that, over a short time window, the pool of asynchronous presynaptic cells fire sparsely (see Gerstner et al. (2014) for detailed explanations).

### 3.1.2 Fast Noise's Large Filtering Timescale

In contrast to Ostojic et al. (2009), we described the fast noise as colored (and not white). This choice was motivated by the result that, in this noise regime, spiking neurons are able to detect subtle input signal changes on the microsecond timescale, despite a typical millisecond-order membrane time constant (i.e., high-frequency encoding; see Gerstner et al. (2014); Ostojic et al. (2015); Tchumatchenko et al. (2011) for extensive review of the theory, and experimental support). More precisely, the LIF neuron's spiking response to a deterministic transient input becomes instantaneous if the timescale of the colored noise is large enough compared to the membrane's time constant (Brunel et al., 2001). In our model, this implies that even in the high noise regime ( $\sigma \sim 10\text{mV}$ ), the PSTH shown in Figure 3 would reflect the shape of the postsynaptic current (PSC) and not of the PSP, making it sharper regardless of the noise variability. Additionally, such a property makes possible the generation of nonstationary and co-modulatory firing with LIF neurons by simply controlling the input current, since the cell firing response follows this current instantaneously. From a physiological standpoint, the "color" of the noise originates from the intrinsic kinetics of the input synapses (Fourcaud and Brunel, 2002; Gerstner et al., 2014). The timescale of the noise is determined by the decay time constants of the synaptic input currents (i.e., PSC's half-width) – a 10 ms timescale can reflect the predominance of GABA<sub>A</sub> receptors.

### 3.1.3 Slow Noise

The slow input noise processes are an important distinguishing characteristic of the biophysical models we have studied here. These processes model synaptic inputs apart from the monosynaptic connection of interest, and are intended to exemplify synchronous network rhythms, such as gamma oscillations, as well as (unobservable) nonstationary background processes. This is the 'background activity' in which the modeled cells are embedded (Buzsáki, 2006) and which acts as a source of coupling. A principal modeling assumption, underlying the plausibility of monosynaptic inference in nonstationary conditions, is that the dominant frequency (more generally, timescale) of such background processes is much slower than the synaptic spike transmission rate ( $\sim 200\text{Hz}$ ) – this is the so-called timescale separation hypothesis (Fujisawa et al., 2008).

The choice of the slow (piecewise constant) input function is an expression of these ideas, and relates pedagogically to the null hypothesis of the jitter test. This null hypothesis is that, conditioned on the spike *counts* in the ( $\Delta$  – length) intervals, all placements of spikes are equally likely (Amarasingham et al., 2012). Thus the hypothesis is one of conditional uniformity, and it is the interval length that specifies the timescale of the process. The generality of this hypothesis stems from the fact that no assumptions are placed on the distribution of spike counts (in the intervals) themselves, which can be generated by processes of arbitrary complexity. Thus the piecewise constant input function is intended as a dynamical source of the statistical (conditional) uniformity. The stochastic mechanism that generates the constants (the  $\mu_k$ 's in Equation 4) is simply a demonstration of arbitrary complexity. Here, we used such discontinuous inputs only for mathematical and pedagogical simplicity.

But, continuous input processes are more biophysically plausible and should be considered in further work. To show the robustness of our principal conclusions to continuous input processes, we replicated our main results using continuous stochastic processes (see the Appendix for the details and results of these simulations).

### 3.1.4 Fast Adaptive Spike Threshold

As opposed to Ostojic et al. (2009), the threshold of our LIF model is dynamic and follows the membrane potential on a fast timescale (Platkiewicz and Brette, 2011; Fontaine et al., 2014; Mensi et al., 2016). As shown by these last authors, the threshold's fast adaptation affects synaptic integration by reducing the effective timescale of somatic integration, enhancing the cell's coincidence detection property. More precisely, a LIF neuron with dynamic threshold can be seen as equivalent to a LIF neuron with fixed threshold but sharper PSPs (Platkiewicz and Brette, 2011; Mensi et al., 2016) – their sharpness scales with the threshold time constant. Several authors argued that sodium channel inactivation is the main factor determining such threshold adaptation *in vivo* (Azouz and Gray, 2003; Henze and Buzsaki, 2001; Wilent and Contreras, 2005; Platkiewicz and Brette, 2011), which received experimental support both *in vitro* and *in vivo* (Fontaine et al., 2014; Mensi et al., 2016). Under this hypothesis, the timescale of threshold dynamics is primarily set by the inactivation time constant around voltage at spike threshold. But more broadly, it is reasonable to interpret fast threshold dynamics as a phenomenological model encompassing various mechanisms that increase the temporal precision of synaptic integration. A standard LIF model, as used by Ostojic et al., can account for a narrow peak in the CCG (see Figure 4 in Ostojic et al. (2009)) but won't account for the sharp millisecond peak observed *in vivo* (see Figure 1E in English et al. (2017)). An additional coincidence mechanism was required for obtaining such a precise spike-spike transmission via a realistic synapse. The fast threshold dynamics is one of the simplest mathematical models to describe an additional coincidence detection component, which is primarily mediated by a robust and effective biophysical mechanism such as fast sodium channel inactivation at the site of action potential initiation.

## 3.2 Alternative Mechanisms for Ultra-precision

Feed-forward inhibition is another mechanism that can explain temporal ultra-precision in pyramidal-to-pyramidal synaptic transmission (Buzsáki, 1984; Pouille and Scanziani, 2001; Isaacson and Scanziani, 2011). Following an excitatory input, a strong and delayed inhibition can prevent the postsynaptic cell from firing a few milliseconds after the excitatory delay, resulting in a millisecond-sharp CCG peak. This mechanism does not contradict our model though, as our assumptions only concern the postsynaptic cell's background input and membrane properties. Adding feed-forward inhibition to our model would presumably make short-latency spike coordination more precise and more robust.

Any biophysical mechanisms known to increase the coincidence detection property of a cell should reinforce the temporal precision of synaptic spike transfer. For example, large average background synaptic conductances (Destexhe et al., 2003) or electrotonic spread between the dendrites and soma (Rall, 1960) can shorten the effective somatic integration timescale, and thus make short-latency spike pairwise coordination tighter.

There are other biophysical mechanisms that give rise to a cell's high-frequency encoding property (and therefore a sharp CCG) than the one considered. Richardson and Swarbrick (2010) and Droste and Lindner (2017) showed theoretically that non-Gaussian noise (i.e.,

synchronous state with large excitatory jumps as observed in DeWeese and Zador (2006); Tan et al. (2014)) can create an ultra-fast cell's response to an input signal current, regardless of the noise timescale. Eyal et al. (2014) and Ostojic et al. (2015) highlighted a similar effect using white noise-driven two-compartment neuron modeling, supposed to abstract the interplay between soma and dendrites *in vivo*. In a more general framework where action potential initiation is explicitly modeled, such as the exponential integrate-and-fire neuron, these results about high-frequency encoding will be all the more pronounced to the degree that spike initiation is sharper (Fourcaud-Trocmé et al., 2003).

### 3.3 Jitter Background Timescale

We showed in this study that the excess synchrony originating from a monosynaptic connection can be accurately estimated, provided that the underlying slow background input timescale is known. But in practice we have, at best, a coarse understanding of this timescale. To better characterize the effect of the assumed timescale on estimation results, we replicated the experiment and analysis underlying Figure 4 while varying the jitter interval length ( $D_\mu/4$ ,  $D_\mu/2$ ,  $D_\mu$ ,  $2D_\mu$ ,  $4D_\mu$ ,  $10D_\mu$ , and the whole trial duration,  $D_{\text{trial}}$ ). As shown in Figure 7A, the closed-form estimate matches the true count as long as the interval length ( $\Delta$ ) is less than or equal to the slow background input timescale,  $D_\mu$ . If the jitter length exceeds this timescale, the estimate agrees with the qualitative trend of the true value, but is clearly biased. Interestingly, in this experiment, jittering at 0.1 or at 10,000 seconds does not result in a significantly different estimate. This experiment suggests that the smaller the value of the jitter interval length,  $\Delta$ , the more confident we will be that the estimate is accurate, so long as the dynamics of monosynaptic transmission justifies the timescale separation ( $\Delta > 5$  ms).

Regarding testing, the statistical power of the jitter test will also depend on  $\Delta$ . To illustrate this, we replicated the experiment and analysis of the previous section ('Parametric Methods'), fixing the number of injected spikes at 50 and varying the jitter interval lengths ( $\Delta \approx D_\mu - 1$ ,  $D_\mu$ , or  $D_\mu + 1$ ). The result of this new experiment is shown in Figure 7B. We observe that the greater the jitter timescale, the greater the power of the jitter test. This is again intuitive; comparing among nested null hypotheses, increasing  $\Delta$  further restricts the null hypothesis (Harrison et al., 2015). The combination of the last two numerical experiments confirms that there is an optimal jitter timescale that controls the trade-off between estimation bias and the test power:  $\Delta$  should be low enough so that the synaptic strength is well estimated for any correctly detected synapse; but large enough to control the false detection rate.

### 3.4 Toward a Theory of Single Trial Data Analysis

Systems neuroscientists are concerned that in typical data-analytical problems conventional approaches to aggregating statistical information across trials, such as averaging, do not apply (Amarasingham et al., 2006; Churchland et al., 2007; Gao and Ganguli, 2015). A more detailed look at this concern reveals the fundamental issue is often overly simplified, even ill-defined, noise models (Amarasingham et al., 2015). The Gaussian noise-driven LIF neuron is a case in point. The application of conditional modeling to timescale specification was designed to address such issues. However, this framework can abstract away the biophysical foundations of spike train models, confounding properties that are typically understood in biophysical terms (Gao and Ganguli, 2015).

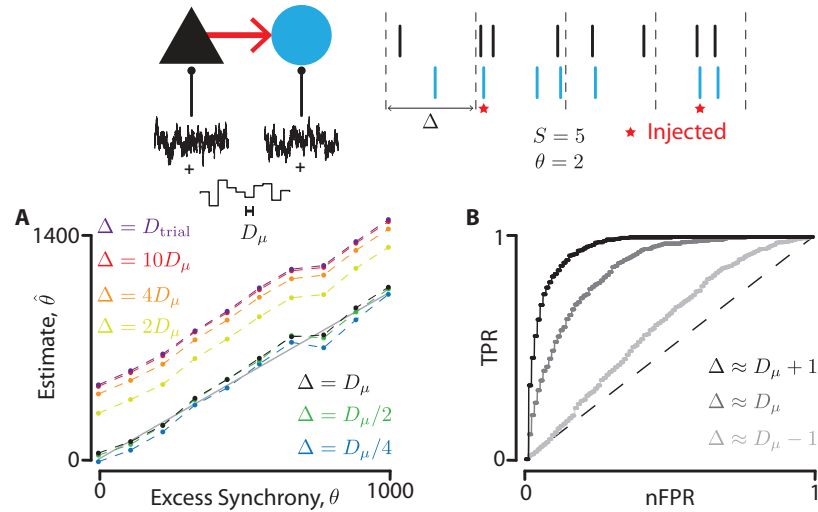


**Fig 7 What is the optimal jitter background timescale?** Spike train pairs were generated using the monosynapse model with spike injection. **A:** In the numerical experiment of Figure 4, we partitioned time into intervals of various lengths for spike resampling ( $\Delta \in \{D_{\mu}/4, D_{\mu}/2, \dots, D_{\text{trial}}\}$ ), and estimated the excess synchrony for each of these partitions. The different partitions are indicated with different colors. Recall that the piecewise constant input's interval length is  $D_{\mu} = 10\text{ms}$ . The gray solid line indicates the first diagonal ( $y = x$ ). **B:** In the numerical experiment of Figure 6, we varied the jitter interval length and computed a ROC curve for each of these values. A gray scale was used to differentiate the different jitter partitions.

We can anticipate a hierarchy of models, at varying levels of physiological detail. Towards this development, the single- and two-timescale models here could be extended to account for the multiple timescales characterizing background network activity, as emphasized by Buzsáki (2006). The biophysical models presented here, and numerous biologically-plausible variations (Gerstner et al., 2014), might be incorporated into the statistical analysis of large-scale extracellular spike data, to further constrain the inference of microcircuit connectivity diagrams. Such a combination may address the issue of overly constrained noise models, and other challenges. As one potentially-fruitful example in this vein, it has been suggested that population spike activity cannot be summarized by independent pairwise spike cross-correlations (Schneidman et al., 2006; Pillow et al., 2008; Gerhard et al., 2013), a mismatch proposed to arise from local connectivity patterns (e.g., triplet connectivity (Song et al., 2005; Jiang et al., 2015; Cossell et al., 2015)).

## 4 Methods

### 4.1 Biophysical Modeling

#### 4.1.1 Single Neuron

The firing dynamics of a cortical neuron was simulated using a leaky integrate-and-fire model with a fast adaptive threshold – an inactivating leaky integrate-and-fire neuron (iLIF) (Platkiewicz and Brette, 2011; Mensi et al., 2016). A spike is emitted whenever the neuron's instantaneous membrane potential  $V(t)$  crosses an instantaneous threshold  $V_T(t)$ .

Immediately after spike triggering,  $V$  is reset to a fixed voltage  $V_R$  and can be held to this value for a few milliseconds (i.e., refractory period, which was not considered in our simulations). Between two spikes, the dynamics of  $V$  and  $V_T$  are linear,

$$\tau_T \frac{dV_T}{dt} = -V_T + f(V), \quad (10)$$

$$\tau_m \frac{dV}{dt} = -V + I, \quad (11)$$

where the voltage  $I$  is the neuron's input; the function  $f(V) = V_{T0} + \alpha \max(0, V - V_i)$  is rectified linear, with  $V_{T0}$  and  $V_i$  the baseline threshold and the inactivation voltage, respectively; the parameters  $\tau_m$  and  $\tau_T$  are respectively the passive membrane time constant and the threshold time constant. The dynamics of  $I$  was described using an Ornstein-Uhlenbeck process,

$$\tau_I \frac{dI(t)}{dt} = -I(t) + \mu(t) + \sigma \sqrt{2\tau_I} \xi(t), \quad (12)$$

where the stochastic term  $\xi$  is a Gaussian white noise of zero mean and unit variance. For two times  $t$  and  $t'$ , we have  $E[\xi(t)\xi(t')] = \delta(t' - t)$ , with  $\delta$  the Dirac Delta function. The parameters  $\tau_I$  and  $\sigma$  are respectively the colored noise's time constant and standard-deviation. To incorporate a nonstationary drive, the time-dependent variable  $\mu(t)$  was made stochastic. It was modeled as a piecewise constant function on equal-length intervals of size  $D_\mu$ ,

$$\mu(t) = \sum_{i=1}^m \mu_i \mathbb{1}\{(i-1)D_\mu \leq t < iD_\mu\},$$

where  $m$  is the number of intervals of size  $D_\mu$  in the trial, and the values  $(\mu_1, \dots, \mu_m)$  were independently and uniformly sampled in  $[\mu_{\min}, \mu_{\max}]$ . We have, as a result,

$E[I(t)I(t')] = \mu_i \mu_j + \sigma^2 \exp(-|t' - t|/\tau_I)$ ,  $t$  and  $t'$  belonging respectively to the  $i$ 'th and  $j$ 'th intervals. It is important to note that the membrane potential,  $V$ , fluctuates around the mean of  $I$ ,  $(\mu_{\min} + \mu_{\max})/2$ , whose value is typically between  $V_R$  and  $V_{T0}$ .

#### 4.1.2 Background Co-Modulation

The model of firing co-modulation between two cortical neurons was a simple extension of the single neuron one. The equations of  $V$  and  $I$  for both neurons were the same as Eqs. 11 and 12, except that there are here two independent white noise terms,  $\xi_1$  and  $\xi_2$ , denoting by the indices 1 and 2 the two neurons of the pair. We have therefore for two times  $t$  and  $t'$ ,  $E[\xi_1(t)\xi_2(t')] = 0$ , but  $E[I_1(t)I_2(t')] = E[\mu(t)\mu(t')]$  since the two neurons share the same exact input mean. In other words, the cross-correlation function of  $I_1(t)$  and  $I_2(t)$  is completely determined by the auto-correlation function of  $\mu(t)$ .

#### 4.1.3 Monosynaptic Transmission

Monosynaptic coupling between two neurons was modeled as in Ostojic et al. (2009) using an input conductance,  $g_s$ . The membrane equation becomes,

$$\tau_m \frac{dV}{dt} = -V + I + \frac{g_s}{g_l} (V - E_s), \quad (13)$$

with  $E_s$  the synaptic reversal potential – if  $V = E_s$ , the synapse has no influence on  $V$ . The synaptic conductance is instantaneously incremented by an amount  $g_0$  after the transmission

of each presynaptic spike, characterized by a fixed delay,  $\delta_s$ . Between two spikes, its dynamics is linear,

$$\tau_s \frac{dg_s}{dt} = -g_s. \quad (14)$$

Following a presynaptic spike emission at time  $t_0$ , we have  $g_s(t) = g_0 \exp(- (t - t_0 - \delta_s) / \tau_s) \mathbb{1}\{t \geq t_0 + \delta_s\}$ .

## 4.2 Numerical Simulations

All simulations of biophysical neuron models were performed using Brian, a spiking neural network simulator in Python (Goodman and Brette, 2008). The spike cross-correlograms were computed using the corresponding function provided in phy, an open source neurophysiological data analysis package in Python (Rossant et al., 2016). For the remaining simulations and generated data analysis, we used NumPy and SciPy (numeric and scientific modules of Python). All the codes used to produce the main results will be available online (<https://github.com/jplatkiewicz/monosynapse-dynamics>).

### 4.2.1 Model Parameters

**Table 1** Biophysical Parameters Values.

Parameters	Pyramidal	Interneuron	Poisson
$\tau_m$ (ms)	10	–	–
$V_R$ (mV)	–60	–	–
$V_i$ (mV)	–60	–	–
$\tau_I$ (ms)	10	–	$\sim 0$
$D_\mu$ (ms)	10	–	5
$\mu_{\max}$ (mV)	–45	–	–35
$\mu_{\min}$ (mV)	–55	–	–45
$\tau_s$ (ms)	×	3	×
$\delta_s$ (ms)	×	1.5	–
$E_s$ (mV)	×	0	×
$\tau_T$ (ms)	1	7	$\sim \infty$
$V_{T0}$ (mV)	–55	–57	–50
$\alpha$	1	0.75	0
$\sigma_I$ (mV)	6	2	5

‘–’ : same value as in the column to the left; ‘×’ : not applicable.

### Spike count computation

In all but Figure 6, synchrony was computed by first partitioning time into bins of a certain width (1 ms except for Fig. 5 where it was 5 ms). The spike trains were then binned (i.e., 1 if any spikes in the bin, 0 otherwise). If for a given bin, a spike was observed in each train of the pair, a synchrony is counted. Obviously, we previously shifted the postsynaptic train leftward by the number of bins corresponding to the implemented synaptic latency.

In Figure 6, we computed first the cross-correlogram between the reference and target trains. The synchrony count is then the sum of the raw spike count in each CCG time bin (of 0.1 ms width) over a window centered around the CCG peak (of 5 ms width).

The ACG's and CCG's were normalized by dividing the spike count in each time bin by the number of reference spikes and the bin width. Under stationary conditions, the normalized count would represent the target cell's instantaneous firing rate relative to a reference spike time.

### 4.3 Semiparametric Analysis of Spike Trains

As described in the main text, a spike train,  $\mathbf{R}$  for example, is modeled in discrete time, and we write  $\mathbf{R} = (R_1, \dots, R_{|\mathbf{R}|})$ , where  $R_i$  is the time of the  $i$ 'th spike in  $\mathbf{R}$ , and  $|\mathbf{R}|$  is the number of elements in  $\mathbf{R}$ . Time is partitioned into equal-length intervals of size  $\Delta$ , and the spike counts in  $\mathbf{T}$  in the intervals are denoted  $\mathbf{N}(\mathbf{R}) = (N_1(\mathbf{R}), \dots, N_m(\mathbf{R}))$  where  $m$  is the number of intervals (Amarasingham et al., 2012).

Here the trains  $\mathbf{R}$  and  $\mathbf{T}$  will be referred to as the reference and target, respectively. In addition, we impose the condition that all intervals that contain a spike in  $\mathbf{T}$  also contain a spike in  $\mathbf{R}$ . (Spikes in the target train that do not satisfy this condition are not in  $\mathbf{T}$ .)

Given two spike trains  $\mathbf{R}$  and  $\mathbf{T}$ , their synchrony count is defined as

$$S = \sum_{i=1}^{|\mathbf{R}|} \sum_{j=1}^{|\mathbf{T}|} \mathbb{1}\{T_j - R_i = \text{lag}\}, \quad (15)$$

where  $\text{lag} \geq 0$  represents the synaptic delay in units of time bins. (The discretization specifies the resolution of synchrony.) In practice, one of the pair of spike trains can be shifted so that the lag can effectively be treated as 0, which is the practice we adopted in this study.

#### 4.3.1 Injected Synchrony Model

When evaluating a cell pair that is putatively monosynaptic, the candidate presynaptic train is chosen as the reference spike train and the candidate postsynaptic one as the target. In the following, we will assume the reference train to be fixed and the target train is random. That is, the probability distribution on  $\mathbf{T}$  operated on here is in fact the conditional probability distribution on  $\mathbf{T}$ , given  $\mathbf{R}$ . The model (“injected synchrony”) is that, conditioned on  $\mathbf{R}$ , the target train  $\mathbf{T}$  is a superposition of two point processes: an “injected” train,  $\mathbf{I}$ , and a “background” train,  $\mathbf{B}$ .  $\mathbf{B}$  is assumed to be conditionally uniform, conditioned on  $\mathbf{N}(\mathbf{B})$  and  $\mathbf{R}$ .  $\mathbf{T} = \mathbf{B} + \mathbf{I}$ , where  $+$  denotes superposition (of point processes). Note that two spikes can be in the same bin in the superposition, which is an approximation. All of the spikes in  $\mathbf{I}$ , on the other hand, are assumed to be synchronous with  $\mathbf{R}$ .

In the following, we will assume the reference train to be fixed and the target train to be random (i.e., we are reasoning conditionally on the reference). The injected synchrony model is that (conditioned on the reference train  $\mathbf{R}$ ), the target train  $\mathbf{T}$  is a superposition of two point processes: an “injected” train,  $\mathbf{I}$ , in which every spike is synchronous with a reference spike; a “background” train,  $\mathbf{B}$ , that is in the  $\Delta$ -jitter null. ( $\mathbf{B}$  is conditionally uniform, conditioned on  $\mathbf{N}(\mathbf{B})$  and  $\mathbf{R}$ .)  $\mathbf{T} = \mathbf{B} + \mathbf{I}$ . Note that in this model two spikes can be in the same bin in the superposition. We think of the latter as an approximation.

The estimation problem is to infer the number of injected synchronies,  $\theta = |\mathbf{I}|$ , where  $'|.|'$  indicates the number of elements in a set. Reasoning conditionally (or parametrically, in

the case of  $\theta$ ), we treat  $\theta$  and  $\mathbf{R}$  as fixed, and we will assume that the background timescale  $\Delta$  is known.<sup>4</sup>

We will use the following notation:

1. Let  $W_i$  identify the interval (with respect to the interval partition) in which target spike  $T_i$  falls. We will collect these as  $\mathbf{W} = (W_1, W_2, \dots, W_{|\mathbf{T}|})$ .
2. Let  $N_{r,i}$  denote the number of spikes in the reference train in window  $W_i$ . We will collect these as  $\mathbf{N}_r = (N_{r,1}, N_{r,2}, \dots, N_{r,|\mathbf{T}|})$ .  $\mathbf{N}_r$  is a function of  $\mathbf{R}$  and  $\mathbf{W}$ . (Note that, by virtue of  $\mathbf{T}$ 's construction,  $N_{r,i} > 0$  for all  $i$ .)
3. Let  $\ell_i$  take the value 1 if spike  $T_i$  is an injected spike (derived from  $\mathbf{I}$ ), let it take the value 0 if it is a background spike (derived from  $\mathbf{B}$ ). We will collect these as  $\mathcal{L} = (\ell_1, \ell_2, \dots, \ell_{|\mathbf{T}|})$ . We have  $\theta = |\mathcal{L}|$ .

Making use of this notation (cf., footnote 4), we can compute

$$E[S|\mathbf{W}, \mathbf{R}, \mathcal{L}] = \theta + \sum_{i=1}^{|\mathbf{T}|} \frac{N_{r,i}}{\Delta} \mathbb{1}\{\ell_i = 0\}. \quad (16)$$

We develop two approaches to estimating  $\theta$ .

#### Case I [ $\mathbf{R}$ 'Homogeneous' ]

Assume that  $\mathbf{R}$  is 'homogeneous,' in the sense that non-zero values of  $N_{r,i}$  are constant (not to be confused with homogeneity in the sense of stationarity).<sup>5</sup> In this case, denote  $\bar{r}$  as  $(1/|\mathbf{T}|) \sum_{i=1}^{|\mathbf{T}|} N_{r,i}$ . The principal example is the sparse case where  $N_{r,i} = 1$  when non-zero (or approximately so), which will generally be more relevant for low firing rates and small  $\Delta$ . In this case,  $E[S|\mathbf{W}, \mathbf{R}, \mathcal{L}] = \theta + \frac{\bar{r}}{\Delta} (|\mathbf{T}| - \theta)$  independently of  $\mathcal{L}$ . Thus

$$E[S|\mathbf{W}, \mathbf{R}] = \theta + \frac{\bar{r}}{\Delta} (|\mathbf{T}| - \theta). \quad (17)$$

Rearranging, we have

$$\frac{E[S|\mathbf{W}, \mathbf{R}] - \frac{\bar{r}}{\Delta} |\mathbf{T}|}{1 - \frac{\bar{r}}{\Delta}} = \theta \quad (18)$$

Taking expectations on both sides:

$$E \left[ \frac{S - \frac{\bar{r}}{\Delta} |\mathbf{T}|}{1 - \frac{\bar{r}}{\Delta}} \right] = \theta, \quad (19)$$

where we have used the fact that  $\bar{r}$  is determined by  $(\mathbf{W}, \mathbf{R})$ , and the general fact that  $f(Z)E[X|Z] = E[f(Z)X|Z]$ , for any random variables  $X, Z$  and function  $f$ . So that (under homogeneity)

$$\hat{\theta}_h = \frac{S - \frac{\bar{r}}{\Delta} |\mathbf{T}|}{1 - \frac{\bar{r}}{\Delta}} \quad (20)$$

<sup>4</sup> For intuition, consider the conceptually simpler special case that an interval consists of two bins, with at most one spike per train in any interval. Then a little thought shows that the problem of estimating  $\theta$ , conditioned on the interval counts, corresponds to the following coin-tossing problem: consider a sequence of  $M$  tosses (corresponding to the number of intervals) involving two coins, one of the coins is fair (corresponding to background spikes) and the other coin is two-headed (corresponding to injected spikes). Let  $\theta$  be the number of tosses of the two-headed coin (corresponding to the number of injected spikes), which is unknown. The problem is, having observed  $H$  heads (synchronies) in the  $M$  tosses, how to estimate  $\theta$ ? Observe that  $E[H] = \theta + \frac{M-\theta}{2}$ . Then simple rearrangement and intuition suggests the natural estimator  $\hat{\theta} = 2H - M$ . Indeed it is equally easy to see that, among other properties,  $\hat{\theta}$  is unbiased (i.e.,  $E[\hat{\theta}] = \theta$ ). This is the essential idea, mapped into the setting of the conditional inference.

<sup>5</sup> Since  $\mathbf{R}$  is in fact observable, this is a potential observation rather than an assumption.

is an unbiased estimator of  $\theta$ .

In the absence of homogeneity, and using a similar idea, estimators that are bounded below and above  $\theta$  in expectation can be constructed by optimizing  $E[S|\mathbf{W}, \mathbf{R}, \mathcal{L}]$  over  $(\theta, \mathcal{L})$ . We do not develop this approach here, but in the Appendix we sketch the construction of confidence intervals for  $\theta$  using that line of thought.

**Case II [ All labellings equally likely. ]**

Suppose, conditioned on  $(\mathbf{W}, \mathbf{R})$ , all  $\mathcal{L}$  are equally likely (LEL) in the sense that

$$P(\mathcal{L}|\mathbf{W}, \mathbf{R}) = \binom{|\mathbf{T}|}{\theta}^{-1} \mathbb{1}\{|\mathcal{L}| = \theta\}. \quad (21)$$

Then define

$$\bar{r} := \frac{1}{|\mathbf{T}|} \sum_{i=1}^{|\mathbf{T}|} N_{r,i}. \quad (22)$$

Explicit calculation shows that

$$E[S|\mathbf{W}, \mathbf{R}] = \theta + \frac{\bar{r}}{\Delta} (|\mathbf{T}| - \theta). \quad (23)$$

Then, using the analogous reasoning from Case I, we obtain

$$\hat{\theta}_{LEL} = \frac{S - \frac{\bar{r}}{\Delta} |\mathbf{T}|}{1 - \frac{\bar{r}}{\Delta}} \quad (24)$$

as an unbiased estimator of  $\theta$  (under LEL).

Note that, in the homogeneous case,  $\hat{\theta}_{LEL} = \hat{\theta}_h$  (i.e., whenever they are both well-defined).

#### 4.3.2 A Bootstrap Confidence Interval For Injected Synchrony

We want to obtain an  $\alpha$ -level confidence interval for the injected synchrony count  $\theta$ . We seek lower and upper bounds  $\theta_{\text{low}}$  and  $\theta_{\text{up}}$ , such that  $\Pr(\theta \in [\theta_{\text{low}}, \theta_{\text{up}}]) \geq 1 - \alpha$ . One can construct a so-called bootstrap interval by generating an empirical distribution of  $\theta$  estimates by bootstrap resampling, and computing the  $100\alpha/2$ 'th and  $100(1 - \alpha/2)$ 'th percentiles of this distribution. More precisely, a bootstrap estimate of  $\theta$  can be computed based on the observed reference train and a bootstrap surrogate target train. This surrogate train can be obtained by resampling the observed target spikes under the injected synchrony model, the equally likely labeling assumption, and an initial estimate of  $\theta$  computed from the observed train pair.

In practice, we implement the following procedure: (1) compute  $\hat{\theta}$  using Eq. 24, based on the observed reference and target trains,  $\mathbf{r}$  and  $\mathbf{t}$ , and a reasonable choice for the jitter interval length  $\Delta$ ; (2) select at random  $\hat{\theta}$  synchronies among all the observed synchronies – we call  $\tilde{\mathbf{I}}$  the selected train and  $\tilde{\mathbf{B}}$  the remaining spike train; (3)  $\Delta$ -jitter  $\tilde{\mathbf{B}}$ , leaving  $\tilde{\mathbf{I}}$  intact (we call  $\mathbf{T}^{(j)} = \tilde{\mathbf{B}}^{(j)} + \tilde{\mathbf{I}}$  a surrogate target train, with  $\tilde{\mathbf{B}}^{(j)}$  the jittered train); (4) compute  $\hat{\theta}^{(j)}$  using Eq. 24, based on the original reference train and the surrogate target train,  $\mathbf{r}$  and  $\mathbf{t}^{(j)}$  (for the same interval length); (5) repeat steps (2)-(4) a large enough number of times,  $N$ , which gives a collection  $(\hat{\theta}^{(1)}, \dots, \hat{\theta}^{(N)})$ ; (6) compute the  $100\alpha/2$ 'th and  $100(1 - \alpha/2)$ 'th percentiles,  $\theta_{\text{low}}$  and  $\theta_{\text{up}}$ , based on the collection obtained in (5).  $[\theta_{\text{low}}, \theta_{\text{up}}]$  is the bootstrap confidence interval.

#### 4.4 Analysis of *in vivo* data

Details for the labeling of ground truth (English et al., 2017) data, and the formation and interpretation of jitter acceptance bands (Amarasingham et al., 2012) can be found elsewhere. In short, exact pointwise acceptance bands are derived by generating  $N_{surr}$  Monte Carlo surrogate CCGs from spike times that are interval-jittered in contiguous and disjoint intervals of duration  $\Delta$ . The surrogate CCG values are ranked for each lag, and pointwise acceptance bands are formed as the region containing the center  $(1 - \alpha) \cdot N_{surr}$  surrogate values per lag. Exact simultaneous acceptance bands are more conservative and control the probability of *any* false rejections, across all lags. Pointwise bands can be interpreted as an appropriate hypothesis test if a hypothesis concerning a particular lag is warranted prior to examination of the data. Simultaneous bands control for the examination of multiple lags. Both acceptance bands are shown in Figure 1B for example neuron pairs. CCGs were discretized to 0.1 ms bins. Simultaneous bands were used as a threshold to detect significant interactions from noise in Figure 1C. The classifiers in the top panels of Figure 1C were the proportion of the CCG exceeding the upper simultaneous band and the number of bins exceeding the upper simultaneous band (both at  $\alpha = 0.05$ -level tests). Curves in Figure 1C were computed via Monte Carlo with 1,000 simulations for each point on each curve. Curves were subsequently smoothed with a window of width eleven samples. Each classifier was used in ROC analyses relative to the ground truth labels provided by the original experiment (English et al., 2017).

#### Conflict of interest

The authors declare that they have no conflict of interest.

#### References

Amarasingham A, Chen TL, Geman S, Harrison MT, Sheinberg DL (2006) Spike count reliability and the poisson hypothesis. *Journal of Neuroscience* 26(3):801–809

Amarasingham A, Harrison MT, Hatsopoulos NG, Geman S (2012) Conditional modeling and the jitter method of spike resampling. *Journal of Neurophysiology* 107(2):517–531

Amarasingham A, Geman S, Harrison MT (2015) Ambiguity and nonidentifiability in the statistical analysis of neural codes. *Proceedings of the National Academy of Sciences* 112(20):6455–6460

Aviel Y, Gerstner W (2006) From spiking neurons to rate models: A cascade model as an approximation to spiking neuron models with refractoriness. *Physical Review E* 73(5):051908

Azouz R, Gray CM (2003) Adaptive coincidence detection and dynamic gain control in visual cortical neurons *in vivo*. *Neuron* 37(3):513–523

Barthó P, Hirase H, Monconduit L, Zugaro M, Harris KD, Buzsáki G (2004) Characterization of neocortical principal cells and interneurons by network interactions and extracellular features. *Journal of neurophysiology* 92(1):600–608

Brody CD (1999) Correlations without synchrony. *Neural computation* 11(7):1537–1551

Brunel N, Chance FS, Fourcaud N, Abbott L (2001) Effects of synaptic noise and filtering on the frequency response of spiking neurons. *Physical Review Letters* 86(10):2186

Buzsáki G (1984) Feed-forward inhibition in the hippocampal formation. *Progress in Neurobiology* 22(2):131–153

Buzsáki G (2006) *Rhythms of the Brain*. Oxford University Press

Churchland MM, Abbott L (2012) Two layers of neural variability. *Nature Neuroscience* 15(11):1472

Churchland MM, Byron MY, Sahani M, Shenoy KV (2007) Techniques for extracting single-trial activity patterns from large-scale neural recordings. *Current opinion in neurobiology* 17(5):609–618

Cossell L, Lacaruso MF, Muir DR, Houlton R, Sader EN, Ko H, Hofer SB, Mrsic-Flogel TD (2015) Functional organization of excitatory synaptic strength in primary visual cortex. *Nature* 518(7539):399

Csicsvari J, Hirase H, Czurko A, Buzsáki G (1998) Reliability and state dependence of pyramidal cell–interneuron synapses in the hippocampus: an ensemble approach in the behaving rat. *Neuron* 21(1):179–189

Date A, Bienenstock E, Geman S (1998) On the temporal resolution of neural activity. In: *Society for Neuroscience Abstracts* (Brown University, Division of Applied Mathematics)

Destexhe A, Rudolph M, Paré D (2003) The high-conductance state of neocortical neurons in vivo. *Nature Reviews Neuroscience* 4(9):739

DeWeese MR, Zador AM (2006) Non-gaussian membrane potential dynamics imply sparse, synchronous activity in auditory cortex. *J Neurosci* 26(47):12206–12218

Droste F, Lindner B (2017) Exact results for power spectrum and susceptibility of a leaky integrate-and-fire neuron with two-state noise. *Physical Review E* 95(1):012411

Dupret D, O'Neill J, Csicsvari J (2013) Dynamic reconfiguration of hippocampal interneuron circuits during spatial learning. *Neuron* 78(1):166–180

English DF, McKenzie S, Evans T, Kim K, Yoon E, Buzsáki G (2017) Pyramidal cell–interneuron circuit architecture and dynamics in hippocampal networks. *Neuron* 96(2):505–520

Eyal G, Mansvelder HD, de Kock CP, Segev I (2014) Dendrites impact the encoding capabilities of the axon. *Journal of Neuroscience* 34(24):8063–8071

Fontaine B, Peña JL, Brette R (2014) Spike-threshold adaptation predicted by membrane potential dynamics in vivo. *PLoS Computational Biology* 10(4):e1003560

Fourcaud N, Brunel N (2002) Dynamics of the firing probability of noisy integrate-and-fire neurons. *Neural Comput* 14(9):2057–2110

Fourcaud-Trocmé N, Hansel D, Van Vreeswijk C, Brunel N (2003) How spike generation mechanisms determine the neuronal response to fluctuating inputs. *The Journal of Neuroscience* 23(37):11628–11640

Fujisawa S, Amarasingham A, Harrison MT, Buzsáki G (2008) Behavior-dependent short-term assembly dynamics in the medial prefrontal cortex. *Nature neuroscience* 11(7):823–833

Gao P, Ganguli S (2015) On simplicity and complexity in the brave new world of large-scale neuroscience. *Current opinion in neurobiology* 32:148–155

Gerhard F, Kispersky T, Gutierrez GJ, Marder E, Kramer M, Eden U (2013) Successful reconstruction of a physiological circuit with known connectivity from spiking activity alone. *PLoS Computational Biology* 9(7):e1003138

Gerstner W (2000) Population dynamics of spiking neurons: fast transients, asynchronous states, and locking. *Neural Computation* 12(1):43–89

Gerstner W, Naud R (2009) How good are neuron models? *Science* 326(5951):379–380

Gerstner W, Kistler WM, Naud R, Paninski L (2014) *Neuronal dynamics: From single neurons to networks and models of cognition*. Cambridge University Press

Goodman D, Brette R (2008) Brian: a simulator for spiking neural networks in python. *Frontiers in Neuroinformatics* 2(5):1–10

Harrison MT, Amarasingham A, Kass RE (2013) Statistical Identification of Synchronous Spiking, spike timing: mechanisms and function edn, CRC Press, chap 4, pp 77–120

Harrison MT, Amarasingham A, Truccolo W (2015) Spatiotemporal conditional inference and hypothesis tests for neural ensemble spiking precision. *Neural computation* 27(1):104–150

Henze D, Buzsaki G (2001) Action potential threshold of hippocampal pyramidal cells in vivo is increased by recent spiking activity. *Neuroscience* 105(1):121–130

Herrmann A, Gerstner W (2001) Noise and the psth response to current transients: I. general theory and application to the integrate-and-fire neuron. *Journal of Computational Neuroscience* 11(2):135–151

Herrmann A, Gerstner W (2002) Noise and the psth response to current transients: II. integrate-and-fire model with slow recovery and application to motoneuron data. *Journal of Computational Neuroscience* 12(2):83–95

Isaacson JS, Scanziani M (2011) How inhibition shapes cortical activity. *Neuron* 72(2):231–243

Jiang X, Shen S, Cadwell CR, Berens P, Sinz F, Ecker AS, Patel S, Tolias AS (2015) Principles of connectivity among morphologically defined cell types in adult neocortex. *Science* 350(6264):aac9462

Jun JJ, Steinmetz NA, Siegle JH, Denman DJ, Bauza M, Barbarits B, Lee AK, Anastassiou CA, Andrei A, Aydin Ç, et al. (2017) Fully integrated silicon probes for high-density recording of neural activity. *Nature* 551(7679):232–236

Kass RE, Eden UT, Brown EN (2014) Analysis of neural data, vol 491. Springer

Kass RE, Amari SI, Arai K, Brown EN, Diekman CO, Diesmann M, Doiron B, Eden UT, Fairhall AL, Fiddament GM, et al. (2017) Computational neuroscience: Mathematical and statistical perspectives. *Annual Review of Statistics and Its Application* 5:183–214

Marshall L, Henze DA, Hirase H, Leinekugel X, Dragoi G, Buzsáki G (2002) Hippocampal pyramidal cell-interneuron spike transmission is frequency dependent and responsible for place modulation of interneuron discharge. *Journal of Neuroscience* 22(2):RC197

Martin AB, von der Heydt R (2015) Spike synchrony reveals emergence of proto-objects in visual cortex. *Journal of Neuroscience* 35(17):6860–6870

Mensi S, Hagens O, Gerstner W, Pozzorini C (2016) Enhanced sensitivity to rapid input fluctuations by nonlinear threshold dynamics in neocortical pyramidal neurons. *PLoS Computational Biology* 12(2):e1004761

Miyawaki H, Diba K (2016) Regulation of hippocampal firing by network oscillations during sleep. *Current Biology* 26(7):893–902

Ostojic S (2011) Interspike interval distributions of spiking neurons driven by fluctuating inputs. *Journal of Neurophysiology* 106(1):361–373

Ostojic S, Brunel N, Hakim V (2009) How connectivity, background activity, and synaptic properties shape the cross-correlation between spike trains. *The Journal of Neuroscience* 29(33):10234–10253

Ostojic S, Szapiro G, Schwartz E, Barbour B, Brunel N, Hakim V (2015) Neuronal morphology generates high-frequency firing resonance. *The Journal of Neuroscience* 35(18):7056–7068

Pillow JW, Shlens J, Paninski L, Sher A, Litke AM, Chichilnisky E, Simoncelli EP (2008) Spatio-temporal correlations and visual signalling in a complete neuronal population. *Nature* 454(7207):995–999

Platkiewicz J, Brette R (2011) Impact of fast sodium channel inactivation on spike threshold dynamics and synaptic integration. *PLoS Computational Biology* 7(5):e1001129

Platkiewicz J, Stark E, Amarasingham A (2017) Spike-centered jitter can mistake temporal structure. *Neural computation*

Pouille F, Scanziani M (2001) Enforcement of temporal fidelity in pyramidal cells by somatic feed-forward inhibition. *Science* 293(5532):1159–1163

Quilichini P, Sirota A, Buzsáki G (2010) Intrinsic circuit organization and theta–gamma oscillation dynamics in the entorhinal cortex of the rat. *The Journal of Neuroscience* 30(33):11128–11142

Rall W (1960) Membrane potential transients and membrane time constant of motoneurons. *Experimental Neurology* 2(5):503–532

Richardson MJ, Swarbrick R (2010) Firing-rate response of a neuron receiving excitatory and inhibitory synaptic shot noise. *Physical Review Letters* 105(17):178102

Rossant C, Leijon S, Magnusson AK, Brette R (2011) Sensitivity of noisy neurons to coincident inputs. *Journal of Neuroscience* 31(47):17193–17206

Rossant C, Kadir SN, Goodman DF, Schulman J, Hunter ML, Saleem AB, Grosmark A, Belluscio M, Denfield GH, Ecker AS, et al. (2016) Spike sorting for large, dense electrode arrays. *Nature Neuroscience* 19(4):634

Schneidman E, Berry MJ, Segev R, Bialek W (2006) Weak pairwise correlations imply strongly correlated network states in a neural population. *Nature* 440(7087):1007–1012

Shahidi N, Andrei AR, Hu M, Dragoi V (2019) High-order coordination of cortical spiking activity modulates perceptual accuracy. *Nature neuroscience* 22(7):1148

Sirota A, Montgomery S, Fujisawa S, Isomura Y, Zugaro M, Buzsáki G (2008) Entrainment of neocortical neurons and gamma oscillations by the hippocampal theta rhythm. *Neuron* 60(4):683–697

Smith MA, Kohn A (2008) Spatial and temporal scales of neuronal correlation in primary visual cortex. *Journal of Neuroscience* 28(48):12591–12603

Song S, Sjöström PJ, Reigl M, Nelson S, Chklovskii DB (2005) Highly nonrandom features of synaptic connectivity in local cortical circuits. *PLoS Biology* 3(3):507–519

Stevens CF, Zador AM (1996) When is an integrate-and-fire neuron like a poisson neuron? In: *Advances in neural information processing systems*, pp 103–109

Tan AY, Chen Y, Scholl B, Seidemann E, Priebe NJ (2014) Sensory stimulation shifts visual cortex from synchronous to asynchronous states. *Nature* 509(7499):226–229

Tchumatchenko T, Malyshev A, Wolf F, Volgshev M (2011) Ultrafast population encoding by cortical neurons. *The Journal of Neuroscience* 31(34):12171–12179

Ventura V, Cai C, Kass RE (2005) Trial-to-trial variability and its effect on time-varying dependency between two neurons. *Journal of Neurophysiology* 94(4):2928–2939

Wasserman L (2013) *All of statistics: a concise course in statistical inference*. Springer Science & Business Media

Watson BO, Levenstein D, Greene JP, Gelinas JN, Buzsáki G (2016) Network homeostasis and state dynamics of neocortical sleep. *Neuron* 90(4):839–852

Wilent WB, Contreras D (2005) Stimulus-dependent changes in spike threshold enhance feature selectivity in rat barrel cortex neurons. *Journal of Neuroscience* 25(11):2983–2991

Yu J, Ferster D (2013) Functional coupling from simple to complex cells in the visually driven cortical circuit. *The Journal of Neuroscience* 33(48):18855–18866

## Supporting information

S1 Appendix: Robustness of the results to a more realistic common input

To illustrate a more realistic point process, we replicated some of the numerical experiments performed in the main study but used instead a continuous slow background input,  $\mu(t) =$

$\mu_0 + \sigma_0 X(t)$ , with  $\mu_0 = -50$  mV,  $\sigma_0 = 2.5$  mV, and  $X$  a stochastic process described by the following dynamics,

$$\begin{aligned} D_\mu \frac{dX}{dt} &= -X + Y, \\ D_\mu \frac{dY}{dt} &= -Y + \sqrt{2D_\mu} \xi, \end{aligned} \tag{1}$$

where  $Y$  is another stochastic process and  $\xi$  is a Gaussian white noise of zero mean and unit variance. These differential equations are arbitrary but incorporate an Ornstein-Uhlenbeck process that is commonly used for modeling synaptic noise. They were also designed so that the timescale  $D_\mu$  is dominant while remaining simple enough. The results are shown in Figure 8, and show similar trends as the results for the experiments with a piecewise constant input. This suggests that our conclusions are robust to shared synaptic input described by a more physiologically realistic process.

## S2 Appendix: Tuning of biophysical parameters

The passive membrane parameters' values were chosen following Ostožić et al. (2009). We took the same value for the membrane time constant,  $\tau_m$ . The reset potential,  $V_R$ , was fixed at 10mV above the resting potential, which we set at its typical value,  $-70$ mV. The refractory period was not taken into account. Similarly, the monosynapse parameters' values were taken from Ostožić et al. (2009). But, we only took a value typical of an excitatory synapse for the reversal potential,  $E_s$ . The input parameters' values were chosen within the commonly accepted physiological range (Gerstner et al., 2014). The mean input was set so that it is around the average voltage threshold, which was set to be about 20mV above the resting potential, as in Ostožić et al. (2009). Such a mean value allows the input variability to have more control on the output firing variability. The input variance of the pyramidal cell was tuned so that it produces an irregular firing typical as observed *in vivo* ( $CV \sim 1$ ). In the interneuron, the input variance was chosen so that it is as low as possible while not preventing irregular firing to happen (as explained in the main text, irregular firing in the interneuron is mostly due to the slow noise component,  $\mu(t)$ ). The amplitude of the slow noise component,  $\mu_{\min}$  and  $\mu_{\max}$ , were chosen so that they are symmetric around the mean input and such that the interneuron's firing is irregular enough ( $CV \sim 1$ ). The input's time constant,  $\tau_I$ , was chosen based on theoretical and empirical considerations (Brunel et al., 2001; Fourcaud and Brunel, 2002; Gerstner et al., 2014). We tuned it large enough compared to the membrane time constant so that the input  $\mu(t)$  had a strong impact on the instantaneous spike rate; but small enough so that it affected as little as possible the input variance on the membrane timescale (for comparison,  $\tau_I \sim 0$  in Ostožić et al. (2009) as the authors studied a white noise input). The active threshold parameters' values were chosen according to the experimental values (Fontaine et al., 2014; Mensi et al., 2016), taking into account the underlying biophysical constraints (Platkiewicz and Brette, 2011). The tuning of these parameters was straightforward for the pyramidal cell since there was no requirement on its coincidence detection property in the context of our study. In addition to the empirical and biophysical conditions, the only criteria that we used was that the cell spiked at its typical firing rate and that the spike autocorrelogram resembled the one observed *in vivo*. The parameter tuning was more intricate for the interneuron. The threshold time constant,  $\tau_T$ , was taken at its lowest plausible value to maximize the coincidence detection effect. The ratio of activation to inactivation slope factors,  $k_a/k_i$ , was fixed around its typical empirical

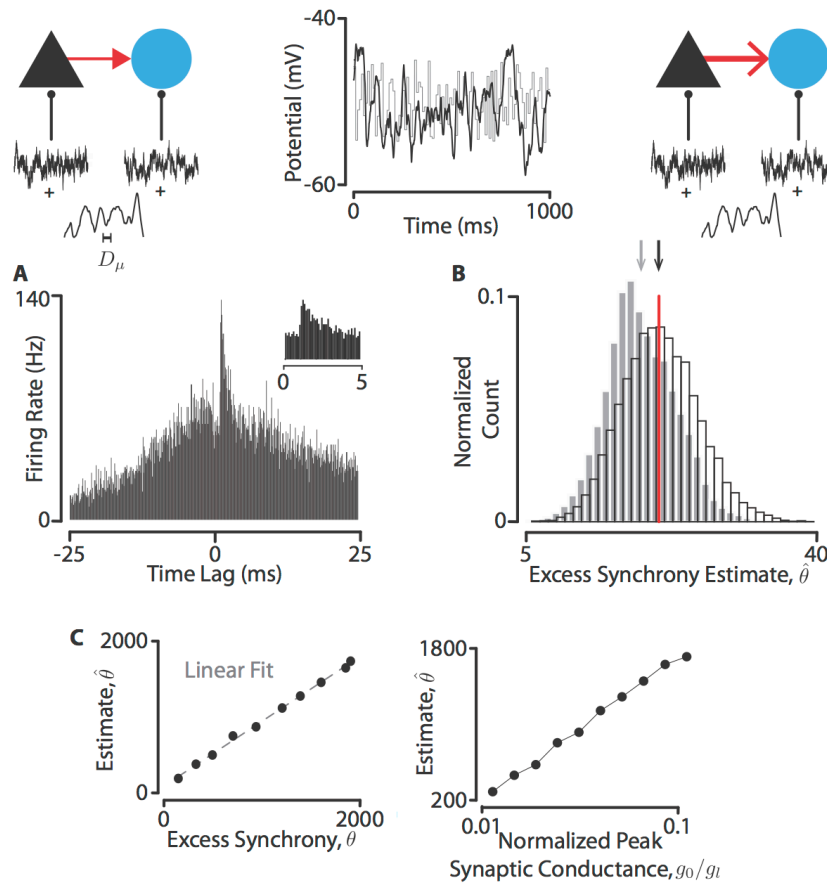


**Fig 8 A smooth common input leads to the same qualitative results** The common input was generated using the system of equations 1. An example is shown in black in the top middle panel (superposed onto a piecewise constant input that was used in the main study, in light gray). The panels A and C were generated using the monosynapse model with a realistic coupling conductance, whereas the panel B was produced using the monosynapse model with artificial spike injection. **A:** Same numerical simulation as in Fig. 3C. The cross-correlogram between the pre- and postsynaptic spike trains exhibits a sharp peak at short latency, similar to the model with a piecewise constant input (see Fig. 3C). **B:** Same numerical experiment and analysis as in Fig. 4A. The black bars indicate the result for the closed-form excess synchrony estimate, whereas the gray bars indicate the result for the “naive” estimate. The closed-form estimate is closer to the true value (red) than the naive one. **C:** Same numerical experiment and analysis as in Fig. 5A (but each trial was three times longer). The black dots indicate the results of the experiment for each value of the monosynaptic conductance. The dashed line represents the result of a linear regression. The solid lines between the markers have been represented to emphasize the relationship. The results are similar to the experiment with piecewise constant input (see Fig. 5A).

value, but making sure it was low enough to allow firing in a standard input regime while being large enough to maximize coincidence detection. The voltage-independent threshold,  $V_{T0}$ , was tuned within a physiologically realistic range but making sure it was low enough compared to the mean input,  $\mu$ , so that firing is possible in a normal input regime while being large enough compared to  $V_i$  for a maximal coincidence detection effect.

S3 Appendix: Sketch of confidence intervals for  $\theta$ .

Here is a sketch of a general approach to constructing a confidence interval for  $\theta$  based on these ideas. The basic idea is to construct hypothesis tests for null hypotheses of the form  $H_0 : \theta = j$ , and then to invert those tests to form a confidence interval for  $\theta$ .

Compute

$$c^+(\mathbf{W}, \mathbf{R}, j) := \arg \min_k \left\{ k \left| \max_{\{\mathcal{L} \mid |\mathcal{L}|=j\}} P(S \geq k | \mathbf{W}, \mathbf{R}, \mathcal{L}) \leq \alpha/2 \right. \right\} \quad (2)$$

and

$$c^-(\mathbf{W}, \mathbf{R}, j) := \arg \max_k \left\{ k \left| \max_{\{\mathcal{L} \mid |\mathcal{L}|=j\}} P(S \leq k | \mathbf{W}, \mathbf{R}, \mathcal{L}) \leq \alpha/2 \right. \right\} \quad (3)$$

It follows that  $\{S \geq c^+(\mathbf{W}, \mathbf{R}, j)\} \cup \{S \leq c^-(\mathbf{W}, \mathbf{R}, j)\}$  is a critical region for an  $\alpha$ -level test of  $H_0 : \theta = j$ .

Then invert the tests. The set

$$C(S, \mathbf{W}, \mathbf{R}, \alpha) = \{j \mid c^-(\mathbf{W}, \mathbf{R}, j) \leq S \leq c^+(\mathbf{W}, \mathbf{R}, j)\} \quad (4)$$

is a (contiguous)  $(1 - \alpha)$ -level confidence interval for  $\theta$  in the sense that

$$P(\theta \in C(S, \mathbf{W}, \mathbf{R}, \alpha)) \geq 1 - \alpha. \quad (5)$$

It turns out that the confidence interval  $C(S, \mathbf{W}, \mathbf{R}, \alpha)$  can be computed efficiently because, in brief, i) the optimizations over  $\mathcal{L}$  in the above expressions are straightforward and independent of  $k$ , ii)  $\max_{\{\mathcal{L} \mid |\mathcal{L}|=j\}} P(S \geq k | \mathbf{W}, \mathbf{R}, \mathcal{L})$  and  $\max_{\{\mathcal{L} \mid |\mathcal{L}|=j\}} P(S \leq k | \mathbf{W}, \mathbf{R}, \mathcal{L})$  can be computed exactly by (fast) convolution, and iii) there is a way to rearrange the computations so that (2) and (3) do not have to be computed independently for each  $j$ . The validity of the intervals do not require stronger assumptions of the model.

It also turns out that, in analogy to the estimation problem and using similar ideas, shorter exact (and contiguous) confidence intervals can also be computed by invoking the LEL assumption. Thus, in addition, both intervals are simultaneously useful in the sense that their discrepancy can be used to measure the effect of the LEL and homogeneity assumptions. The details of these procedures are outside the scope of this study and will be reported elsewhere.

## S4 Appendix: Jitter and bootstrap sensitivity; some calculations

As elsewhere, condition on the reference train, so we are jittering the target train.  $\Delta$  is fixed. Denote by  $M$  the number of intervals containing at least one spike in both trains. The goal is to compare surrogate generation methods with respect to sensitivity of departures from the null detected by the synchrony statistic. Denote by  $n_{t,i}$  the number of spikes for the target train in window  $i$ . Let  $k_i$  be the number of bins in window  $i$ , which will contribute to the synchrony count upon containing a target spike (note this depends only on the reference train, and the definition of synchrony width). Then let us call  $Y_i^{b/s}$  the synchrony count from a bootstrap surrogate,  $Y_i^{b/s}$  the synchrony count from window  $i$  in a bootstrap surrogate.  $Y^{b/s} = \sum_{i=1}^M Y_i^{b/s}$ .  $Y^j$  and  $Y_i^j$  are, analogously, from a jitter surrogate. Let  $\mathbf{N}$  be the interval counts. Then notice that

$$E[Y^{b/s} | \mathbf{N}] = E[Y^j | \mathbf{N}]. \quad (6)$$

Also,

$$\sum_{i=1}^M \frac{n_{t,i}}{\Delta} \left(1 - \frac{n_{t,i}}{\Delta}\right) k_i = \text{Var}[Y^{b/s}|\mathbf{N}] \quad (7)$$

$$> \text{Var}[Y^j|\mathbf{N}] \quad (8)$$

$$= \sum_{i=1}^M \frac{n_{t,i}}{\Delta} \left(1 - \frac{n_{t,i}}{\Delta}\right) k_i \underbrace{\frac{\Delta - k_i}{\Delta - 1}}_{\text{Hyperg. c.f.}} \quad (9)$$

(The hypergeometric correction factor is the correction factor for sampling with, as opposed to without, replacement; analogous quantities give similar relationships in the continuum.)

Let us translate observations into standard deviations with respect to the common mean of the bootstrap and jitter distributions. Suppose the observed synchrony is  $\tilde{x}$ .

$$\frac{\frac{\tilde{x} - E[Y^{b/s}|\mathbf{N}]}{\sqrt{\text{Var}[Y^{b/s}|\mathbf{N}]}}}{\frac{\tilde{x} - E[Y^j|\mathbf{N}]}{\sqrt{\text{Var}[Y^j|\mathbf{N}]}}} = \frac{\sqrt{\text{Var}[Y^j|\mathbf{N}]}}{\sqrt{\text{Var}[Y^{b/s}|\mathbf{N}]}} = \frac{\sqrt{\sum_{i=1}^M \frac{n_{t,i}}{\Delta} \left(1 - \frac{n_{t,i}}{\Delta}\right) k_i \frac{\Delta - k_i}{\Delta - 1}}}{\sqrt{\sum_{i=1}^M \frac{n_{t,i}}{\Delta} \left(1 - \frac{n_{t,i}}{\Delta}\right) k_i}} \quad (10)$$

It is instructive to consider constant  $n_{t,i} = t$  and  $k_i = k$  examples. Then

$$\frac{\text{Std}[Y^j|\mathbf{N}]}{\text{Std}[Y^{b/s}|\mathbf{N}]} = \frac{\sqrt{\sum_{i=1}^M \frac{n_{t,i}}{\Delta} \left(1 - \frac{n_{t,i}}{\Delta}\right) k_i \frac{\Delta - k_i}{\Delta - 1}}}{\sqrt{\sum_{i=1}^M \frac{n_{t,i}}{\Delta} \left(1 - \frac{n_{t,i}}{\Delta}\right) k_i}} = \sqrt{\frac{\Delta - k}{\Delta - 1}}, \quad (11)$$

where  $\text{Std}$  denotes standard deviation. That is, in the constant  $t, k$  case, if  $\tilde{x}$  is  $m$  standard deviations from the mean with respect to the jitter distribution, it is  $\sqrt{\frac{\Delta - k}{\Delta - 1}}m$  standard deviations from the the mean with respect to the bootstrap distribution. This provides an explanation of the finer sensitivity of the jitter test, in the case of a synchrony test statistic. Note the key quantity involves  $k/\Delta$ .

## S5 Appendix: A necessity argument for interval jitter tests of conditional uniformity

Let  $\mathbf{X}$  be the spike train(s) and  $\mathbf{N} = \mathbf{N}(\mathbf{X})$  be the interval counts. Suppose that the null hypothesis is that  $\mathbf{X}$  is conditionally uniform, given  $\mathbf{N}$ . Suppose one has a level  $\alpha$  test of the null hypothesis specified by critical region  $C$ . Then it follows that

$$\Pr(C|\mathbf{N} = \mathbf{n}) \leq \alpha \forall \mathbf{n}, \quad (12)$$

because otherwise one can obtain a contradiction.<sup>6</sup>

This suggests that, taking the conditional uniformity null for granted, any test is equivalent to a permutation test. We can see that the test determined by  $C$  must be equivalent to a (deterministic) permutation test specified by a test statistic  $T(\cdot)$ . Define  $C_k = C \cap \{\mathbf{N} = \mathbf{k}\}$ . Let

$$T(\mathbf{X}) = \mathbb{1}\{\mathbf{X} \in C_{\mathbf{N}(\mathbf{X})}\}. \quad (13)$$

<sup>6</sup> Suppose it is not true. Then there is a  $\mathbf{n}'$  such that  $\Pr(C|\mathbf{N} = \mathbf{n}') > \alpha$ . But then consider the distribution satisfying  $\mathbf{X}$  uniform on the set  $\{\mathbf{N}(\mathbf{X}) = \mathbf{n}'\}$ . This distribution is both in the null and yields  $\Pr(C) > \alpha$ .

It follows that

$$C_{T(\mathbf{X}),\alpha} = \{\mathbf{X} : T(\mathbf{X}) \geq 1\} = C, \quad (14)$$

where  $C_{T(\mathbf{X}),\alpha}$  is the level- $\alpha$  deterministic permutation (i.e., interval jitter) test induced by statistic  $T(\cdot)$ . (The Monte Carlo version coincides with this deterministic test in the limit as the number of surrogates goes to  $\infty$ .)